HHS Public Access

Author manuscript

Nat Metab. Author manuscript; available in PMC 2024 December 13.

Published in final edited form as:

Nat Metab. 2023 December ; 5(12): 2131–2147. doi:10.1038/s42255-023-00919-3.

Inhibition of the proline metabolism rate-limiting enzyme P5CS allows proliferation of glutamine-restricted cancer cells

Samantha J. Linder[1,#], **Tiziano Bernasocchi**[1,9,#,*], **Bárbara Martínez-Pastor**[1,^], **Kelly D. Sullivan**[2,3], **Matthew D. Galbraith**[2,9], **Caroline A. Lewis**[4], **Christina M. Ferrer**[1,10], **Ruben Boon**[1,10,$], **Giorgia G. Silveira**[1,10], **Hyo Min Cho**[1,10], **Charles Vidoudez**[11], **Stuti Shroff**[5], **Joao P. Oliveira-Costa**[1,10,@], **Kenneth N. Ross**[6], **Rami Massri**[8], **Yusuke Matoba**[12,13], **Eugene Kim**[12,13], **Bo R. Rueda**[12,13], **Shannon L. Stott**[1,7,10], **Eyal Gottlieb**[8,%], **Joaquin M. Espinosa**[2,9], **Raul Mostoslavsky**[1,9,*]

[1]The Krantz Family Center for Cancer Research, the Massachusetts General Hospital Cancer Center, Harvard Medical School, Boston, Massachusetts 02114, USA

[2]Linda Crnic Institute for Down Syndrome, University of Colorado Anschutz Medical Campus, Aurora, CO 80045, USA

[3]Section of Developmental Biology, Department of Pediatrics, University of Colorado Anschutz Medical Campus, Aurora CO 80045, USA

[4]The Whitehead Institute for Biomedical Research, Massachusetts Institute of Technology, Cambridge MA 02139, USA

[5]Department of Pathology, The Massachusetts General Hospital, Harvard Medical School, Boston, Massachusetts 02114, USA

[6]Dana Farber Cancer Institute, Harvard Medical School, Boston, MA 02115, USA

[7]Center for Engineering in Medicine and Surgery, The Massachusetts General Hospital, Dept. of Medicine, Harvard Medical School, Boston, MA 02114

[8]The Ruth and Bruce Rappaport Faculty of Medicine, Technion-Israel Institute of Technology, Haifa, Israel

[*]Corresponding authors: rmostoslavsky@mgh.harvard.edu, tbernasocchi@mgh.harvard.edu.
[^]Current Address: Spanish National Cancer Research Center (CNIO), Madrid, Spain
[$]Current Address: Galapagos de Wittelaan, 2800 Mechelen, Belgium
[@]Current Address: Takeda Pharmaceuticals, Cambridge MA 02139
[%]Current Address: MD Anderson Cancer Center, Houston TX77030
[#]These authors contributed equally

Author contributions:
S.J.L., T.B., B.M-P., C.M.F., and R.B., C.V., H.M.C, performed the experiments; R. Massri and E.G. generated and analyzed the P5CS CRISPR-KO cells; K.D.S., M.D.G. and J.M.E. provided the shRNA library and performed the analysis of screening data; C.A.L. performed and analyzed the metabolomics assays; K.N.R. analyzed the TCGA data; S.Schroff. provided the patient-derived tumor tissue slides; J.P.O-C., G.G.S. and S. Stott imaged and analyzed the IHC of the tissue slides; Y.M., E.K. and B.R.R. provided deidentified FFPE sections representing endometrial cancer and endometrial cancer cell lysates from the Vincent Center for Reproductive Biology Gynecologic Tissue Repository for analysis. S.J.L, T.B., and R. Mostoslavsky conceptualized and designed the study, analyzed results and wrote the manuscript; R. Mostoslavsky and T.B., supervised the project.

Competing interests:
Authors declare no competing interests.

Tables
Tables S1

[9]Department of Pharmacology, University of Colorado School of Medicine, Anschutz Medical Campus, Denver CO 80204, USA

[10]The Broad Institute of Harvard and MIT, Cambridge MA 02142, USA

[11]Harvard Center for Mass Spectrometry, Cambridge (MA), USA.

[12]Vincent Center for Reproductive Biology, Department of Obstetrics and Gynecology, Massachusetts General Hospital, Boston, MA, 02114, USA

[13]Department of Obstetrics, Gynecology and Reproductive Biology. Harvard Medical School, Boston, MA 02115, USA

Abstract

Glutamine is a critical metabolite to rapidly proliferating cells, as it is used for the synthesis of key metabolites necessary for cell growth and proliferation. Glutamine metabolism has been proposed as a therapeutic target in cancer, and several chemical inhibitors are in development or in clinical trials. How cells subsist when glutamine is limiting is poorly understood. Using an unbiased screen, we identify *ALDH18A1*, which encodes P5CS, the rate-limiting enzyme in the proline biosynthetic pathway, as a gene that cells can downregulate in response to glutamine starvation. Notably, P5CS downregulation promotes de novo glutamine synthesis highlighting a previously unrecognized metabolic plasticity of cancer cells. The glutamate conserved from reducing proline synthesis allows cells to produce key metabolites necessary for cell survival and proliferation under glutamine-restricted conditions. Our findings reveal an adaptive pathway that cancer cells acquire under nutrient stress, identifying proline biosynthesis as a previously unrecognized major consumer of glutamine, a pathway that could be exploited for developing effective metabolism-driven anti-cancer therapies.

Introduction

Cancer cells have massive bioenergetic and biosynthetic needs, and metabolic reprogramming is an effective strategy that provides the energy and biomass required to sustain basic cellular functions and growth, as well as to mitigate oxidative stress. Although glucose metabolism has been extensively researched in cancer, studies in recent years have identified glutamine as a major source of carbon and nitrogen in cancer cells (1). Through its entrance into the TCA cycle, transamination reactions, or as an exchange factor, glutamine critically supports ATP production, NAD synthesis, glutathione-driven reductive power, and biomass intermediates for lipids, amino acids and nucleotides (2). As such, it is not surprising that glutamine is an essential component in the media of most cultured cells, as originally described by Krebs and Eagle (3, 4). This dependency appears to be more important *in vitro*, as *in vivo* studies have shown that certain tumors can instead rely on endogenous synthesis of glutamine (5–8). Whether cells obtain glutamine from extracellular sources or through *de novo* synthesis, glutamine plays a critical role in maintaining cellular viability and proliferation. Particularly in the context of cancer, the rapid proliferation rendered these cells highly dependent on glutamine, and many oncogenic pathways evolved to drive glutamine metabolism, including Myc and KRAS (1, 9). However, despite glutamine being the most abundant amino acid found in circulation (10), several studies

have shown that many solid tumors exhibit extremely low levels of glutamine, compared to their neighboring normal tissues (11–13). This is even more exaggerated in the cores of solid tumors, where high glutamine consumption and poor vascularization results in nutrient scarcity (15, 16). These results suggest that cancer cells can adapt to survive and even proliferate in the context of glutamine deficiency. Furthermore, drugs that target glutamine metabolism are being tested in clinical trials and understanding how cells may adapt and become resistant to such treatments will be critical to effectively treat patients.

While previous studies have determined mechanisms by which cancer cells avoid cell death due to glutamine deprivation (9, 16–17), studies defining adaptations that allow active proliferation have been performed with mixed results (6, 18–21, 7, 22–24, 8, 25). Using an unbiased genome-wide screen, we identified an unreported resistance mechanism by which downregulation of P5CS, the rate limiting enzyme in proline biosynthesis, not only allows glutamine-independent cell survival, but also proliferation in glutamine-deprived media. Downregulation of proline synthesis allows cells to rewire glutamate towards *de novo* glutamine synthesis through glutamine synthetase (GS), as well as other downstream metabolites that altogether support cell survival and proliferation under extreme nutrient scarcity, particularly de novo nucleotide synthesis. Our results indicate a previously unrecognized role for proline biosynthesis as a major consumer of glutamate. As such, proline metabolism may represent an unique vulnerability, and cancer cells that re-wire this pathway to adapt to glutamine restriction could become extremely sensitive to therapy with GS inhibitors.

Results

Genome-Wide Glutamine Deprivation Screen identifies ALDH18A1.

To identify strategies that cells employ to overcome their dependency on glutamine and continue to proliferate, we conducted a genome-wide, glutamine-deprived short-hairpin knockdown screen, using an inducible Myc-overexpressing cell line (MycER MEFs) that is highly addicted to glutamine (9) (Fig.1A, Extended Data Fig. 1A–B). The only source of glutamine in the screen came from the 10% FBS provided in the medium (approximately 50 uM in the final composition of the media), mimicking extreme glutamine deprivation (Extended Data Fig. 1E). This model was extremely robust (i.e., no cell survival of non-transduced cells under glutamine-deprived conditions), preventing false positives in the screen. Strikingly, after ~20 days, actively proliferating clones were observed in the glutamine-free media, transduced plates (Fig. 1B). This polyclonal population was then expanded, and genomic DNA isolated for next-generation sequencing. Analysis of sequencing results from the screen revealed that the control (glutamine) and experimental (glutamine-deprived) conditions clustered separately, and the experimental replicates were robustly consistent, as determined in pairwise sample-sample Euclidean distances clustering (Extended Data Fig. 1C). Most shRNAs were skewed towards depletion (Suppl. Fig. 1D), as expected from the stringent conditions of the screen where most cells died due to failure to adapt to glutamine starvation. Importantly, several shRNAs were significantly enriched, with at least 2 shRNAs passing the designated threshold (Fig. 1C, Table S1). Of these shRNAs, those targeting *Aldh18a1* were the most significantly enriched, identifying this gene as the

top hit (Fig. 1D). *Aldh18a1* is a gene that encodes the mitochondrial enzyme pyrroline-5-carboxylate synthase (P5CS), which catalyzes the *first* step in proline biosynthesis (see below, Fig. 2A) (26). Based on its ranking in the screen, as well as its role in metabolism, this gene was prioritized for further study.

To validate *Aldh18a1* as a genuine target whose downregulation confers glutamine independence, we generated two independent stable-knockdown (KD) lines and subjected these cells to glutamine deprivation (Fig. 1E). Consistent with our screening findings, knockdown of *Aldh18a1* allowed MycER MEFs to proliferate in glutamine deprived media, while the control cells could not (Fig. 1E–F). Notably, *Aldh18a1* CRISPR knockout (KO) lines derived from mouse primary epithelial cells isolated from the kidney were also developed, and while these KO cells grew poorly (they required supplementation with proline to grow efficiently in culture), they also exhibited a growth advantage in glutamine-deprived conditions, particularly in the absence of proline (Extended Data Fig. 1F), providing further validation to our approach.

Importantly, when we cultured these cells in the presence or absence of glutamine long-term (~2 weeks), *Aldh18a1* deficient cells are counter-selected in the presence of glutamine (and grew even poorer in full media compared to WT cells, Extended Data Fig. 1G), indicating that in full media, synthesis of proline provides a survival advantage (Fig. 1G and Extended Data Fig. 1H). In contrast, if cells remained starved of glutamine, they retain the knockdown and continue to select for lower P5CS expression (Fig. 1G; Extended Data Fig. 1H). Altogether, these experiments validated our initial screening and provided conclusive evidence that cells can adapt to glutamine starvation via downregulation of *Aldh18a1* expression.

Downregulation of *Aldh18a1* re-wires Cellular metabolism.

P5CS, the protein encoded by *Aldh18a1*, converts glutamate to pyrroline-5-carboxylate (P5C), an intermediate in the proline biosynthetic pathway, and its downregulation completely inhibit proline production and secretion (26) (Fig. 2A, Extended Data Fig. 2A–B). Because P5CS consumes glutamate in its reaction, we hypothesized that upon knockdown of this enzyme, the cellular pool of glutamate would increase, allowing the shunting of GLU towards other metabolic processes. To start assessing how these cells re-wire metabolism we performed targeted polar LC-MS metabolomics using ^{15}N-labeled ammonia ($^{15}NH_4^+$) in sh*Adh18a1* MycER MEFs cultured in glutamine-restricted media (Fig. 2B–C). Importantly, we detected clear ^{15}N-labeled glutamine in the KD cells exposed to glutamine-free medium, as well as asparagine, hexosamines, and nucleotides, all metabolites that require glutamine for their synthesis (Fig. 2C). Of note, aspartate emerged as the lone metabolite to exhibit downregulation in the shALDH18A1 cells, likely due to its utilization for asparagine and pyrimidine synthesis under these nutrient restrictive conditions (Fig. 2C) (7). Indeed, the elevated asparagine levels coincided with a clear increase in expression of asparagine synthetase (ASNS), the enzyme that catalyzes *de novo* asparagine synthesis (Fig. 2D). These results were quite intriguing, as recent literature has suggested that certain cells can resist glutamine deprivation through increasing asparagine synthesis (7, 17–18). However, supplementing WT cells with 2mM asparagine in glutamine-deprived

conditions failed to rescue proliferation (Fig. 2E). These results reveal that asparagine, at least by itself, is not sufficient to support the proliferation of cells in the context of glutamine restriction.

The above results indicate that de novo synthesis of glutamine from GLU may be key for the proliferation of these cells. In this context, a major mechanism by which cancer cells overcome their dependency on exogenous glutamine is *de novo* glutamine synthesis by glutamine synthetase (GS) (5–8). In its reaction, GS catalyzes the ATP-dependent condensation of free ammonia and glutamate to produce glutamine. Strikingly, chemical inhibition of glutamine synthetase (GS) by L-methionine sulfoximine (MSO) completely blocked *Aldh18a1* KD cells from proliferating in glutamine-deprived media (Fig. 2A and F). Importantly, treatment with an inhibitor of glutaminase (GLS,) CB-839, which converts glutamine into glutamate, affected the growth of both controls and KD cells equally, suggesting that is the re-wiring of glutamate which is critical for these cells to grow (Fig. 2A and F). Altogether, these results indicate that *Aldh18a1*-deficient cells are fully dependent on *de novo* glutamine synthesis to proliferate in glutamine-deprived media.

α-KG dependent survival and nucleotide/asparagine-dependent proliferation requires Glutamine biosynthesis.

The above labeling experiment suggests that nucleotides, asparagine, and hexosamines may represent key nutrients downstream of glutamine that the cells require to support proliferation under these restrictive conditions. However, supplementation with each metabolite alone or in combination did not rescue the proliferation of WT cells in glutamine restricted conditions (Fig. 3A). It is important to note that these resources, while important for proper cell function/proliferation, are metabolites downstream of glutamine that utilize its amide nitrogen, not its carbon backbone (Fig. 2B). Previous studies have shown that carbon sources, such as α-ketoglutarate (α-KG), robustly rescue glutamine starvation-induced cell death (but not proliferation) in the context of Myc amplification by supporting the TCA cycle (9, 16). Therefore, we hypothesized that while these nitrogen sources may be important for cell proliferation, they have no role in inhibiting death, and thus are useless to a dying cell. Indeed, addition of α-KG significantly rescued cell death upon glutamine restriction in WT cells (Fig. 3B, Extended Data Fig. 3A–B). To specifically trace the carbons in the context of sh*Aldh18a1*, we monitored the flux of glutamine under glutamine-limited conditions, employing 500 μM of $^{13}C_5$-GLN (Fig. 3C–D). As anticipated, our data showed a complete cessation of proline synthesis from glutamine. Intriguingly, the sh*Aldh18a1* cells exhibited increase label of glutamine and glutamate, coupled with an increase in TCA cycle intermediates (including α-KG, malic acid, and citric acid). Biomass precursors, encompassing nucleosides and amino acids, were also augmented (Fig. 3C–D). The increase in labeled glutamine was not matched by an increase in media-derived glutamine, further indicating an increase in *de novo* glutamine synthesis from the spare glutamate conserved by the inhibition of proline synthesis (Extended Data Fig. 2B). To complement these experiments, we also performed $^{13}C_5$-GLU labeling. We uncovered a remarkable four-fold surge in de novo glutamine synthesis from labeled glutamate, accompanied by significant contribution to TCA cycle intermediates and nucleosides (Extended Data Fig. 4A–B). Therefore, we decided to supplement WT cells with 7mM α-KG, as described previously

(9). Indeed, α-KG was able to rescue survival (but not proliferation), as compared to stained plates on day 0 of the experiment, before glutamine deprivation (data not shown). Strikingly, combining α-KG with ASN, GlcNAc, and nucleosides completely rescued WT cells' proliferation in glutamine-deprived media (Fig. 3E). Dropout experiments demonstrated that GlcNAc was not required for the rescue (Extended Data Fig. 4C). We next tested whether providing these end-products would bypass the requirement of glutamine, which may still be required for protein synthesis and intermediate metabolism. Treatment of the rescued cells with MSO slightly but significantly affected the rescue (Extended Data Fig. 4D), indicating that a fraction of glutamine, indeed, could be used for other purposes. Altogether, these results indicate that α-KG, ASN, and nucleosides appear to be the critical metabolites supporting cell survival and proliferation in the context of glutamine deprivation (Fig. 3F).

Importantly, we had not ruled out the possibility that by downregulating P5CS, the proline pathway could be biased toward proline catabolism, rather than biosynthesis, therefore providing glutamate from proline breakdown (Fig. 3F). Previous studies have shown that certain cancers, such as pancreatic cancer, can catabolize proline from their extracellular environment to provide a sufficient source of nutrients when others are limited (27). To test this possibility, we knocked down ALDH4A1, which encodes the enzyme opposite to P5CS that converts the metabolite P5C to glutamate (P5C dehydrogenase; P5CDH) (Fig. 3F). If proline is acting as a key source of glutamate, knockdown of both P5CS and P5CDH would inhibit survival and proliferation of these cells in the absence of glutamine. Notably, these cells continued to proliferate in medium lacking glutamine, despite knockdown of both enzymes (Extended Data Fig. 4E). A major limitation of this study is that these *in vitro* experiments were performed using DMEM medium, which lacks proline. The only source comes from the FBS supplemented in the medium (Extended Data Fig. 1E). However, exogenous supplementation of proline, alone or in combination with ASN and nucleosides, did not rescue cell proliferation in glutamine-deprived media (Supp Fig. 4F). Taken together, these results suggest that proline breakdown is not a significant source of carbon and/or nitrogen when glutamine is limiting, but rather the increased availability of glutamate that is maintained by inhibiting the flux towards proline is critical in providing a proliferative advantage.

The observation that proline supplementation did not rescue *Aldh18a1* deficient cells from glutamine starvation was surprising, as we had hypothesized that even if proline is not used to generate glutamate, supplementing with excess proline should inhibit P5CS activity and therefore rescue glutamine deficiency by eliminating a major path by which glutamate is consumed. One explanation could be that rapid conversion of proline into ornithine or arginine could maintain a need for proline and consequently P5CS activity. To investigate this, we tested whether supplementation with all three metabolites (Proline, Ornithine, and Arginine) and NAC could rescue glutamine deprivation. The addition of these amino acids alone or in combination did not rescue glutamine deficiency (Extended Data Fig. 5A). It is also possible that even when proline is in excess, P5CS does not sense it and continues to synthesize proline from glutamate, given the requirement to re-generate mitochondrial NADP+ pools (28–29; see Discussion). We tested this possibility by labeling glutamine and assessing fractional labeling of proline in the excess of unlabeled proline. Indeed, even in the presence of extra proline, we still observed a significant contribution of glutamine to

the pool of proline, which was almost completely inhibited following knockdown of P5CS (Fig. S5B). In line with these findings, supplementation of proline to MycER cells did not alleviate the impact of glutamine deprivation on proliferation, but it did have an effect in full media (Extended Data Fig. 5C–D). Considering both P5CS and P5CRL/1/2 consume NADPH for proline production, we cannot rule out the possibility that the downregulation of the proline synthesis pathway could also avert a detrimental imbalance in the NADPH/NADP+ ratio during glutamine scarcity. To test this hypothesis, we assessed the NADPH/NADP+ ratio, and indeed, the absence of proline synthesis partially preserved the ratio compared to control cells (Fig. S5D).

In summary, our findings identified P5CS as a significant glutamate consumer, stimulating proline synthesis even in conditions of proline surplus and consuming vital NADPH required by cells under glutamine-limited conditions.

Downregulation of P5CS in human cancer cells leads to glutamine resistance and MSO inhibitor sensitivity.

ALDH18A1 has been poorly characterized in the context of human cancer. To start to investigate whether cancer cells could as well modulate *ALDH18A1* as a physiological adaptation to low glutamine, we first analyzed publicly available human tumor data from The Cancer Genome Atlas (TCGA). Notably, we found that low *ALDH18A1* mRNA expression is associated with decreased survival of patients in both endometrial/uterine and stomach cancers (Fig. 4A). This contrasts with patients with lung tumors, as decreased P5CS expression correlated with increased survival (data not shown), consistent with previous studies in lung cancer cells suggesting that inhibition of proline synthesis is detrimental to cell survival (30, 31). A more detailed analysis in endometrial cancer revealed that the lower the expression of P5CS, the poorer overall survival. Further, the decreased expression of P5CS is specifically prevalent in uterine serous carcinoma and stage G3 high-grade endometrial cancer- the most aggressive forms of uterine cancer (Extended Data Fig. 6A–D). These findings suggest that proline metabolism and its relevance in tumorigenesis may be tissue-type dependent, as seen with other metabolic pathways.

To directly determine whether P5CS downregulation could provide an advantage in certain human cancers, we first tested glutamine dependency on several cancer cell lines, and found a range of sensitivities, as expected (Extended Data Fig. 6E). The stomach cancer line NUGC2 and prostate cancer cell line PC3 were chosen as a model for *ALDH18A1* modulation, as they exhibited extreme sensitivity to glutamine deprivation, similar to MycER MEFs (Extended Data Fig. 6E). Notably, following knockdown of P5CS, these cells continued to proliferate in the absence of glutamine, indicating that in human cancer cells (as observed in MEFs), inhibition of P5CS confers a growth advantage in response to glutamine deprivation (Fig. 4B–C; Extended Data Fig. 6F). Moreover, the PC3 cancer cell line mirrored our observations in the MycER cells, where a growth advantage was apparent only under glutamine-limited conditions. However, when the cells were reintroduced to a glutamine-rich environment, this advantage was lost. (Fig. 4C; Extended Data Fig. 6F). We next tested whether we could rescue survival and proliferation of WT NUGC2 cells in low glutamine by providing the key metabolites previously identified. Indeed, supplementation

with α-KG, ASN, and nucleosides resulted in a robust rescue in these cells (Fig. 4D). Lastly, knockdown of P5CS in PC3, NUGC2 and an endometrial cell line (MFE-280), conferred these cells with extreme sensitivity to GS inhibition (MSO) but not to GLS inhibition (CB-389) (Fig. 4E–F; Extended Data Fig. 6F and G), suggesting that, similar to the MycER MEFs, their ability to proliferate in the absence of glutamine is also dependent on *de novo* glutamine synthesis. Taken together, these results indicate that *ALDH18A1* deficiency allows for adaptation to glutamine starvation not just in Myc-amplified MEFs, but also in human cancer cells, thereby representing a robust, evolutionarily conserved, adaptive mechanism. To determine whether downregulation of P5CS provides an advantage *in vivo*, we injected NUGC2 WT and P5CS KD cells into mice. Strikingly, downregulation of P5CS provided a major growth advantage, a phenotype that was fully rescued by re-expression of P5CS (Fig. 4G–H, Extended Data Fig. 7A), ruling out off-target effects. We next performed nitrogen-labeling experiments in these cancer cells, and, similar to what we observed with the MycER MEFs, we saw increased glutamine and nucleotides labeling, indicating that also in cancer cells, P5CS downregulation shifts metabolism towards biomass production (Extended Data Fig. 7B).

Human cancer cells reduce P5CS expression as an adaptation to glutamine restriction.

We next investigated whether cancer cells could regulate endogenous levels of P5CS in response to glutamine deprivation. For this purpose, we subjected several human cancer cell lines to 24 hours glutamine depletion. Surprisingly, out of the 13 lines tested, 4 (31%; EN, MKN45, OCUM-1, VCAP) displayed a clear decrease in P5CS protein upon 24 hours glutamine starvation (Fig. 5A; Extended Data Fig. 7C), indicating that cancer cells may selectively modulate proline metabolism in order to adjust to glutamine deprivation. To investigate whether this adaptation could provide an advantage *in vivo*, we performed xenograft studies with two of these lines. MKN45 and EN cells were pre-conditioned by long-term culture in complete or glutamine-deprived medium, then injected into matching flanks of SCID mice (Fig. 5B). Strikingly, we found that both MKN45 and EN cells pre-cultured in glutamine-deprived medium form larger tumors than their full media counterparts (Fig. 5C). These results are particularly strong, as the glutamine-deprived cells grew slower *in vitro* (compared to complete media controls), suggesting that the *in vivo* setting provides a stressed environment where these adapted cells appear to proliferate better. Additionally, extracts from these tumors revealed that several of them retained lower P5CS levels, despite growing for several weeks *in vivo* (Extended Data Fig. 7D). These results suggest that either these cells retained a memory of the metabolic stress they were previously exposed to *in vitro*, or that the *in vivo* setting was also low in glutamine. To investigate if the glutamine-adapted EN cancer cells, which endogenously downregulated P5CS, also re-wire GLU metabolism, we repeated the $^{15}NH4$ labeling experiment, as we did with the MycER cells (with genetic downregulation of P5CS – Fig. 2F). Based on labeling data, EN_low glutamine cancer cells (EN_LG) upregulated de novo glutamine synthesis and redirected metabolic flux towards asparagine and nucleotide synthesis, as seen in the MycER model (Fig. 5D).

Lastly, we performed immunohistochemistry and immunofluorescence analysis of patient-derived gastric tumor tissues and uterine serous carcinoma (USC) using antibodies against

P5CS and GS (Fig. 5E and G; Suppl. Fig7E). Although staining was variable (indicative of the heterogeneous nature of solid tumors), we found clear intratumor regions where an inverse correlation between P5CS and GS staining was observed (Fig. 5E–H, Extended Data Fig. 7E). It is of particular interest that patches of tumor cells exhibited decreased P5CS and concomitant increased GS, suggesting that tumors may experience glutamine deprivation in a focal manner, and cells can adapt by rewiring proline metabolism. Moreover, consistent with the previous data, USC tumors predominantly showed downregulation of P5CS and overall upregulation of GS (Extended Data Fig. 6A–D and 7F). These findings indicate that the mechanism we discovered in our screen may play an adaptive role in human cancers.

Discussion

Our findings have identified proline metabolism as a key pathway that can be modulated in response to glutamine deprivation. De-prioritization of proline biosynthesis in order to utilize glutamate for other metabolic programs is a previously unrecognized cellular adaptation to survive and grow in glutamine-deprived environments. Furthermore, it indicates that the proline biosynthetic pathway is a major consumer of glutamate, supporting historical studies that identified proline as a significant product of glutamine metabolism (30,31). It is important to note that most of the previous literature has indicated pro-oncogenic roles for proline metabolism (32–36). Contrastingly, our studies suggest that proline biosynthesis can be limiting for tumor growth, specifically in conditions of glutamine restriction, by shunting glutamate away from the synthesis of key metabolites required for cell survival and proliferation. In this context, a recent study has shown that collagen-derived proline was required for the proliferation of pancreatic cancer cells under nutrient-deprived conditions (27). The results from that study indicated that proline was used to replenish TCA cycle intermediates. In our study, we demonstrated that inhibition of proline synthesis instead was required to salvage glutamate and regenerate glutamine to sustain nucleotide biosynthesis and ASN. Surprisingly, the addition of excess proline/ornithine/arginine did not rescue the proliferation defect in low glutamine, indicating that even when proline is freely available, cells continue to synthesize proline from glutamate (Extended Data Fig. 5A). One possibility is that the requirement to re-generate NADP+ through proline cycling (critical to support nucleotides' synthesis through the Pentose-Phosphate Pathway) maintains the pathway even in excess of proline, and therefore the only way cells can salvage glutamate is by inhibiting P5CS, the rate-limiting enzyme in proline biosynthesis that consumes glutamate. In this context, we found that numerous human cancer cell lines downregulate P5CS as a mechanism to adapt against glutamine deprivation, indicating that this response may have evolved as a general mechanism to tolerate metabolic stress. Prior research has demonstrated that the efficacy of glutaminase inhibitors, such as CB-839, positively correlates with proline levels in breast cancer cell lines (47). Conversely, in our study, we observe an inverse pattern of enhanced susceptibility, but in relation to glutamine synthetase (GS) inhibitors, like MSO, when P5CS is downregulated. This heightened sensitivity is coupled with a notable lack of specificity to glutaminase inhibitors, an observation that differs from previous findings.

These results indicate that therapeutic approaches could potentially be customized based on the tumor's proline dependency. The interplay between proline biosynthesis, governed

by P5CS, and the glutamine metabolic pathway, in which both GS and glutaminase (GLS) are key enzymes, presents a previously undocumented paradigm for understanding and exploiting cancer cell vulnerabilities. By manipulating this proline-glutamine metabolic axis, we may be able to influence cancer cell survival and proliferation, tailoring therapies to specific metabolic dependencies. Therefore, monitoring levels of proline and understanding the tumor's reliance on proline synthesis may provide valuable insights into putatively unexplored effective treatments. Additionally, our findings regarding high-grade endometrial cancer suggests that P5CS expression could be used as a determinant in both the prognosis and progression of this disease. In summary, our findings enhance our understanding of cellular metabolic reprogramming, how it contributes to oncogenesis and tumor aggression, as well as inform investigators on potential mechanisms of resistance to glutamine-metabolism inhibition. Importantly, P5CS deficient cells can proliferate in glutamine restriction in a *de novo* glutamine synthesis-dependent manner, suggesting that inhibition of the enzyme glutamine synthetase may prove quite effective in inhibiting these adaptive mechanisms in human tumors.

Methods:

This study was conducted in strict accordance with all relevant ethical guidelines and regulations. Human participants were recruited at Massachusetts General Brigham, and informed consent was obtained from all subjects. The research protocol was reviewed and approved by the Institutional Review Board (IRB) under protocol number #2022P003117.

Cell lines and cell culture

MycER MEFs (gift from Ralph DeBerardinis, UT Southwestern) and human cancer cells FU-97, MKN1, MKN45, OCUM-1, NUGC2, KLE, EN, MFE-280, Ishikawa, VCAP, 22RV1, LNCAP, and PC-3 (gift from Cyril Benes, MGH Center for Cancer research) were grown in high glucose, sodium pyruvate-free, glutamine-free DMEM medium (Gibco) supplemented with 10% FBS (Sigma-Aldrich) and 1% penicillin-streptomycin (10,000 U/mL) (Gibco), with or without 2mM L-glutamine (Gibco) added, as indicated. Cells cultured in DMEM without GLN in the context of regular FBS have a content of glutamine of 50uM (Extended Data Fig.1E) and therefore are named "Glutamine deprived condition/ media." When 2mM of GLN is added to the media mentioned above, this condition is named "complete medium or GLN medium (39)". When specified, the following substances were added individually, or in combination: 1mM MSO (Sigma-Aldrich, M5379), 0.5mM L-proline (Sigma-Aldrich), 2mM L-asparagine (Sigma-Aldrich), 7mM (MycER MEFs) or 3.5mM (human cells) dimethyl-α-ketoglutarate (Sigma-Aldrich, 349631), 15mM N-acetyl-D-glucosamine (Sigma-Aldrich, A3286), 250μM (MycER MEFs) or 125μM (human cells) each cytidine, thymidine, uridine, adenosine and guanosine (Sigma-Aldrich). Unless otherwise mentioned, all stable shRNA knockdown lines were cultured in the presence of 2 μg/mL puromycin (Thermo Fisher Scientific). Fh1fl/fl immortalized kidney epithelial cells were grown in high glucose, sodium pyruvate-free, glutamine-free DMEM medium supplemented with 10% FBS (Gibco), 2mM L-glutamine (Biological Industries),1% penicillin-streptomycin (Biological Industries), and 100 μM sodium pyruvate (Biological Industries). *Aldh18a1*-KO cells (C2-KO and C9-KO), which are derived from Fh1fl/fl cells,

were also supplied with 600μM L-proline (Sigma-Aldrich). All cells were cultured and maintained at 37°C under 5% CO2, and passaged by trypsinization.

shRNA screening, library preparation, and NextGen sequencing

Transduction of MycER MEF cells and library preparation for Illumina sequencing were carried out essentially as previously described (37). In brief:

Pooled shRNA library virus production and infection: A pool of plasmids encoding ~60,000 shRNAs targeting ~15,000 genes (mouse TRC2 library) in the pLKO.1 backbone produced by The RNAi Consortium (TRC, Sigma-Aldrich, St. Louis, MO) were obtained from the University of Colorado Cancer Center Functional Genomics Shared Resource. 12.5μg of mouse TRC2 library DNA was mixed with 12.5μg of packaging virus mix DNA (1:9 ratio of pVSV-G:pΔ8.9) and incubated with Mirus TransIT-293 Transfection Reagent (Mirus Bio) for 20 min at room temperature. This mixture was then added to 6×10^6 HEK293T cells in order to give 100x coverage of the library. Cells were then incubated at 37°C under 5% CO_2 overnight. 12–16 hours post-transfection, medium was changed. 48 hours post-transfection, viral supernatant was collected and filtered through a 0.45μm cellulose acetate filter. The entire viral supernatant was then used to transduce 6×10^6 MycER MEFs (100x coverage, plated between two 15cm plates) with 10 μg/mL polybrene (Millipore Sigma). Two days post-transduction, cells were selected in 2 μg/mL puromycin (Thermo Fisher) for at least 5 days.

Glutamine deprived screening: Screens were performed in three independent biological replicates for each treatment Complete or glutamine deprived media). In brief, 7×10^6 library-infected MycER MEFs were seeded in 2 15cm plates (3.5 million/plate) using complete medium. The next day, cells were washed twice with phosphate-buffered saline (PBS) (Gibco), then medium replaced with complete or glutamine deprived media, and 200μM 4-OHT (Sigma-Aldrich, H7904). Media was changed every 3 days, until colonies were visibly formed in the glutamine deprived plates (~ 10 days). Cells grown with complete media were passaged every 2 to 3 days, always re-plating at least 7 million cells. Colonies growing in glutamine deprived media were left to grow until they could be pooled and expanded to a 10cm plate coated with 0.2% gelatin (~3 weeks). Cells were then further expanded until they filled at least 2, 15cm gelatin-coated plates (~1 week). At the end of the screening (total time: 4–5 weeks), cells were trypsinized, counted, and pelleted into aliquots of 6×10^6 cells per tube for processing.

Illumina HiSeq library construction and nextGen sequencing: Briefly, genomic DNA was isolated from 6×10^6 cell aliquots of both the complete and glutamine deprived conditions selected samples using the Qiagen DNeasy Blood & Tissue kit (Qiagen, 69504). To build the multiplexed sequencing library, the shRNA insertion region was first amplified from 500ng of genomic DNA using Phusion high fidelity DNA polymerase (NEB, M0530), yielding a 497 base pair (bp) PCR product (PCR1). After purification using the Qiagen PCR purification kit (Qiagen, 28104), 1μg of purified PCR1 DNA was digested with XhoI (NEB) overnight at 37°C, which cleaved the stem-loop region. This digestion yielded 2 products (271bp and 226bp). To purify the desired 271bp DNA fragment, the total digestion was

run on a 2.3% agarose gel and the band extracted with the QIAquick Gel extraction kit (Qiagen, 28704). Barcoded linkers, which enable multiplexing of samples, were prepared by annealing single-stranded oligonucleotides purchased from Integrated DNA Technologies (IDT), creating double-stranded linkers with an XhoI overhang. Annealed linkers were run over Illustra MicroSpin G-25 columns (GE Healthcare, 27-5325-1) to remove any remaining single-stranded oligonucleotides. Selected barcoded linkers were then ligated to 100ng of each 271 bp fragment overnight at 16°C. The resulting 312bp ligation product was purified on a 2.3% agarose gel, and gel extracted as described above. Finally, Illumina adapters, which are required for bridge amplification and sequencing, were added by PCR using 10ng of the purified ligation, yielding a PCR product of 144bp (PCR2). The entire PCR reaction was purified on a 2.3% agarose gel and extracted as above. Final samples were quantified using the Qubit dsDNA High Sensitivity Kit (Life Technologies) and pooled in equal amounts to yield the final multiplexed library. Libraries were sequenced on the Illumina HiSeq2500 instrument, resulting in approximately 35 million 50bp reads per sample on average (The MGH NextGen Sequencing Core).

shRNA screen sequencing analysis

Data quality was assessed using FastQC (https://www.bioinformatics.babraham.ac.uk/projects/fastqc/). Reads were demultiplexed, trimmed to remove vector sequence and retain only shRNA sequences, and quality filtered (keeping only reads with quality score ≥10 for ≥19 of 20 bases) using the Fastx toolkit (http://hannonlab.cshl.edu/fastx_toolkit/). Reads were then aligned against an index containing the TRC2 library shRNA sequences using Bowtie2 (38) and counts per shRNA in each sample tabulated. The following steps were carried out in R (v3.6.1) using a custom script with the limma (v.3.40.6), tidyverse (v1.2.1), and ggplot2 (v3.2.0) packages. Reads were then normalized to counts per million (cpm) and batch corrected across replicates using limma::removeBatchEffect and normalized batch corrected counts compared between replicates. Ratios for treatment (no glutamine) / control (glutamine) were calculated for per replicates and the median of three replicates taken as the fold-change for each shRNA.

Threshold-based hits: To score shRNA hits, thresholds of mean cpm >5 in either treatment or control samples and fold-changes of ≥2 for enrichment or ≤0.5 for depletion were applied. To score hits at the gene level, a minimum of two enriched or depleted shRNAs was required.

Rank-sum-based hits: To identify genes for which targeting shRNAs display a significant shift in distribution towards greater fold-changes compared to all shRNAs, two-sample Wilcox tests (aka Mann-Whitney) were carried out for each gene.

TCGA analysis

Human stomach adenocarcinoma and uterine corpus endometroid carcinoma patient tumor data was obtained from TCGA to evaluate the *in vitro* models. TCGA STAD (stomach adenocarcinoma) and UCEC (uterine corpus endometroid carcinoma) RNASeqV2 expression data and the associated clinical information for those samples (TCGA Network, 2015) was downloaded from the TCGA data matrix access portal (http://

cancergenome.nih.gov/). TCGA RNASeqV2 data was downloaded during April 2015 and TCGA clinical data was downloaded during December 2015. Follow-up clinical data files were merged with the original clinical data file to ensure that the most up-to-date patient follow-up information was used for survival analysis. Downloaded TCGA data was loaded into and analyzed in R. There were 363 STAD samples with RNASeqV2 data and clinical information and at least 6 months of clinical follow-up or the patients were dead. There were 155 UCEC samples with HiSeq RNASeqV2 data and clinical information and at least 6 months of clinical follow-up or the patients were dead. The Kaplan-Meier plots and the log-rank p-values using R and used overall survival with death from any cause as the end point and patients still alive at their last follow-up were censored at their last follow-up time. The samples in the Kaplan-Meier plots were split according median log2 *ALDH18A1* expression with median log2 expression values for *ALDH18A1* of 11.39 for STAD and 11.67 for UCEC.

Glutamine *dependency assay*

Human cancer cells were seeded in triplicate in six-well plates in order to reach ~50% confluence the next day in complete medium. The next day, medium was removed, cells washed twice with PBS, and complete or glutamine deprived media added. Four days later, viable cells were trypsinized and counted using trypan-blue exclusion and a hemocytometer. Percent cell survival was calculated using the following equation: (average number of cells in glutamine)/(average number of cells in + glutamine) x 100 = percent survival.

shRNA-mediated knockdown of ALDH18A1

For stable *Aldh18a1* knockdown, pLKO.1-puro vectors containing shRNAs targeting mouse *Aldh18a1* (#1: 5'-CCGGTGTCCAGCCCTCAGCTATTAGCTCGAGCTAATAGCTGAGGGCTGGACATTTTTG-3', #2: 5'-CCGGTAGCTGTGCCCAGATCAAATCCTCGAGGATTTGATCTGGGCACAGCTATTTTTG-3'), human *Aldh18a1* (#1: 5'-CCGGACTTTGCCAAGTCCAATTATCCTCGAGGATAATTGGACTTGGCAAAGTTTTTTG-3', #2: 5'-CCGGTTCACGTTAAACTTGTCTTATCTCGAGATAAGACAAGTTTAACGTGAATTTTTG-3') (MGH Molecular Profiling Lab, MGH Center for Cancer Research), or a non-specific 'scrambled' shRNA (5'-CCGGCCTAAGGTTAAGTCGCCCTCGCTCGAGCGAGGGCGACTTAACCTTAGGTTTTTG-3') were cotransfected into HEK293T cells with expression vectors containing lentiviral packaging (pCMV-Δ8.9) and envelope protein (pCMV-VSV-G) genes using X-tremeGENE™ 9 DNA Transfection reagent (Millipore Sigma). Viral supernatants were harvested 48 hours post-transfection, filtered with a 0.45μm filter, and added to sub-confluent MycER MEFs or NUGC2 cells with 10 μg/mL polybrene (Millipore Sigma) for 12–16 hours. Two days post-infection, cells were selected in 2 μg/mL puromycin for at least 4 days.

CRISPR-mediated knockout of Aldh18a1

sgRNA design: The 20-nucleotide short guide RNA (sgRNA) targeting exon 16 of the *Aldh18a1* gene was designed via the online tool developed by the Zhang research team (Broad Institute/MIT): http://www.genome-engineering.org/crispr/. sgRNA top and bottom strands were commercially supplied by Hylabs as two single-stranded oligonucleotides (Top: 5'-CACCGTCACATTTAGAGTCTCTGAC-3'; Bottom: 5'-AAACGTCAGAGACTCTAAATGTGAC-3'). CACC bases were added to the 5' end of the top strand, and AAAC bases added to the 5' end of the bottom strand in order to create 5' sticky ends complementary to those produced as a result of cutting with the BbsI restriction enzyme. An extra guanine (G) was also added to the 5' end of the 20nt sgRNA sequence, as the U6 RNA polymerase III promoter prefers its transcripts to start with G.

Vector and CRISPR KO Line production: After annealing the oligonucleotide strands and ligating into the PX-459-V2 system (pSPCas9(BB)-2A-Puro; gift from Feng Zhang, The Broad Institute/MIT), the plasmid was transiently transfected into transformed mouse kidney epithelial cells via Lipofectamine™ 3000 Reagent (Thermo Fisher Scientific), using the standard protocol. 24 hours after transfection, cells were treated with 1 μg/mL puromycin for 36 hours. Single-cell clones were then derived via limiting dilution into a 96-well plate. Several colonies were picked and screened for P5CS expression via western blot analysis.

Cell line: Immortalized primary epithelial cells isolated from kidney of $Fh1^{fl/fl}$ mice in which the fumarate hydratase (FH) gene is flanked by LoxP sequences. The cells were isolated, immortalized, and authenticated in Dr. Eyal Gottlieb's former laboratory at the CRUK Beatson Institute in Glasgow, as previously described (40).

P5CS reconstitution

After subcloning *Aldh18a1* cDNA (transcript variant 1) into BamHI and XhoI sites of the pMIGR overexpression vector, which contains an internal ribosomal entry site (IRES)–GFP cassette, (gift from Debbie Yablonski, Technion-Israel Institute of Technology), the vector was transfected into phoenix cells (retrovirus-producing cells derived from HEK293Ts that produce gag-pol and envelope protein), according to the standard calcium phosphate protocol. Viral supernatants were harvested 24 hours post-transfection, filtered with a 0.45μm filter, and added to sub-confluent *Aldh18a1*-KO cells with 8.5 μg/mL polybrene (Mercury) for 16–24 hours. This step was repeated twice. Two days post-infection, cells underwent limiting dilution for ~3 weeks, then GFP expressing single-cell clones selected.

Cell lysis and immunoblotting

Whole cell lysates were prepared by resuspending cells in RIPA lysis buffer (0.5% sodium deoxycholate, 150mM sodium chloride, 1% NP-40, 50mM Tris-HCl pH 8.0, 0.1% SDS, 10% glycerol, 5mM EDTA pH8.0) supplemented with a protease inhibitor cocktail (Complete EDTA-free, Roche Applied Science), 5μM TSA, 5mM sodium butyrate, 1mM DTT, 1mM PMSF, 50mM sodium fluoride, and 0.2mM sodium orthovanadate, and incubated on ice for 20 min. The lysate was then centrifuged at 14,000g for 15min at 4°C, and protein-containing supernatant collected. Chromatin extracts were prepared by resuspending cells in lysis buffer (10mM HEPES pH 7.4, 10mM KCl, 0.05% NP-40)

supplemented with the same components as listed above and incubated on ice for 20min. The lysate was then centrifuged at 14,000g for 10min at 4°C. The supernatant (cytosolic fraction) was removed and the pellet (nuclei) acid-extracted using 0.2N HCl and incubated on ice for 20min. The sample was then centrifuged at 14,000g for 10min at 4°C. The supernatant (containing acid-soluble proteins) was neutralized using 1M Tris-HCl pH 8. Protein concentration for both whole cell lysates and chromatin extracts was measured by the Bio-Rad Protein Assay. Western blot analyses were performed as previously described (41). In brief, 20 μg of whole cell lysate or 10μg of chromatin was loaded on 4–20% gradient polyacrylamide gels with SDS (Bio-Rad) and electroblotted onto polyvinylidene difluoride (PVDF) membranes (Millipore). Membranes were blocked in TBS containing 5% non-fat milk and 0.1% Tween and probed with primary antibodies. The following primary antibodies were used: anti-P5CS (Proteintech, 17719-1-AP, 1:1000), anti-P5CDH (Proteintech, 11604-1-AP, 1:1000), anti-GS (Sigma-Aldrich, G2781, 1:1000), anti-ASNS (Proteintech, 14681-1-AP, 1:1000), anti-MYC (Abcam, ab32072, 1:1000); anti-LDHA (Cell Signaling, 2012S, 1:1000); anti-total H3 (Abcam, ab1791, 1:2000); anti-α-tubulin (Sigma-Aldrich, T6199, 1:2000); and anti-β-actin (Sigma-Aldrich, A5316, 1:2000). Bound proteins were detected with horseradish-peroxidase-conjugated goat anti-rabbit (Vector Laboratories, PI-1000, 1:1000) or anti-mouse (Vector Laboratories, PI-2000. 1:1000) secondary antibodies and developed with ECL (GE Healthcare).

Glutamine starvation/selection experiments:

MycER MEFs or NUGC2 cells were seeded in 6-well plates at 150,000 (MycER MEFs) or 100,000 (NUGC2) cells per well using complete medium. The next day, medium was removed, cells washed twice with PBS, and medium replaced with glutamine deprived media. Media was changed every 2 days for 16–18 days to monitor colony formation. For NUGC2 control and *Aldh18a1* KD cells, number of colonies were counted per well and represented as an average (n=3). Bright-field images were taken using a Leica DMI4000 B microscope. The cells that were actively growing in G glutamine LN deprived conditions were expanded and frozen (now known as sh*Aldh18a1* "select" cells) to be used for subsequent cell growth/proliferation assays. WT and P5CS CRISPR KO mouse kidney epithelial cell lines were seeded in 6-well plates at 30,000 cells per well in complete medium. The next day, medium was removed, cells washed twice with PBS, and medium replaced with complete or GLN deprived media, and with or without 600μM L-proline. Cells with glutamine were grown for 1 week, and those glutamine -free media for 1 month. To quantify growth, cells were washed with PBS, fixed by incubation with methanol for 20 minutes at −20°C, and stained with 0.5% crystal violet for 1 hour. After staining, crystal violet was removed and cells washed with ddH_2O. Plates were dried overnight, imaged, and crystal violet dissolved by addition of 1mL methanol and shaking for 1 hour at 75rpm. Crystal violet was quantified by measuring optical density (OD) at 570nm. For the Pro-Arg-Orn rescue experiment, 5,000 cells were seeded in a 12-well plate in complete medium. The next day, medium was removed, cells washed twice with PBS, and medium replaced with GLN deprived media with the addition of 2mM of Proline, Arginine, and Ornithine. After 5 days, the cells were stained for quantification as mentioned above.

Cell growth/proliferation assays

For all growth/proliferation experiments, cells were seeded in complete medium, allowed to adhere overnight (~8–10 hours), followed by 2 washes with PBS and replaced with complete or GLN deprived media.

Manual counting: Cells were seeded in triplicate in 12-well plates at 40,000 (MycER MEFs) or 60,000 (NUGC2) cells per well. The next day, an initial “day 0” seeding plate was trypsinized and counted using trypan-blue exclusion and a hemocytometer. The remaining plates were washed twice with PBS, and medium replaced with complete or glutamine deprived media. To monitor proliferation, adherent cells were counted every 48 hours for 10 days. Medium was changed every other day throughout the course of the experiment.

Crystal violet staining: Cells were seeded in triplicate as mentioned above. The next day, an initial “day 0” seeding plate was fixed and stained with 25% methanol/0.5% crystal violet for 1 hour, washed 3 times with miliQH_2O, and left to dry overnight. The remaining plates were washed twice with PBS, and medium replaced with complete or glutamine deprived media, plus any other nutrients or chemicals as indicated. Cells were left to grow for 5 days, with medium replaced every other day. On day 5, cells were fixed and stained, washed, and dried as mentioned above. Plates were then imaged and staining quantified using the FIJI software (42, 43). For the CyQUANT single time-point experiment, approximately 10,000 NUGC2 cells were seeded in each well of a 96-well plate. The following day, the culture medium was changed to either normal medium, glutamine-deprived medium, or normal medium supplemented with α-ketoglutarate (αKG), asparagine (ASN), and CTUAG (nucleotides), or a combination of αKG, ASN, and CTUAG. After a period of 5 days, cell proliferation was evaluated using the CyQUANT Cell Proliferation Assay Kit from Thermo Scientific (C7026) in accordance with the manufacturer’s instructions.

Cell Death Assay

Cell death was assessed by Propidium Iodide (PI) staining followed by flow cytometry. MycER and NUGC2 cells were cultured in normal conditions, glutamine-deprived conditions (-glutamine), and glutamine-deprived conditions supplemented with α-Ketoglutarate (-glutamine + α-KG) for 5 days. Cell preparation for PI staining was performed as follows: After 5 days of culture, cells were harvested by trypsinization and washed twice in cold phosphate-buffered saline (PBS). Approximately 1 million cells were resuspended in 500 μL of PBS. Staining procedure: to each cell suspension, 5 μL of PI solution (1 mg/mL, Sigma-Aldrich) was added and incubated in the dark at room temperature for 15 minutes. Following incubation, samples were kept on ice prior to flow cytometry analysis. Flow cytometry analysis: stained cells were analyzed using a flow cytometer. Unstained cells were used as a negative control. Dead cells were identified as PI-positive and quantified using the flow cytometry software. The gating strategy was performed as illustrated in Supplementary Figure 3B-C.

The percentage of PI-positive cells (dead cells) in each sample was recorded and compared between different treatment groups to determine the effects of glutamine deprivation and α-KG supplementation on cell death. All experiments were performed in triplicate.

NADPH/NADP assay

The NADPH/NADP+ ratio was assessed using the NADP/NADPH Assay Kit (ab65349). Approximately 300,000 cells were seeded in each well of a 6-well dish. After allowing cells to adhere, they were treated with either normal medium or medium devoid of glutamine for a period of 48 hours. Following treatment, cells were harvested and processed as per the manufacturer's protocol. The quantification of NADP+ and NADPH levels was then performed according to the provided kit instructions.

MSO and CB-839 inhibitors

In the assays for L-Methionine sulfoximine (MSO) and Telaglenastat (CB-839), approximately 10,000 PC3, EN, MFA, and NUGC2 cells were each seeded in a 96-well plate. The following day, increasing doses of MSO (Sigma #M5379) and CB-839 (Selleck Chemicals #S7655) were added to the wells. The dosages for the MSO inhibitor were 200 mM, 40 mM, 8 mM, 1.6 mM, 0.32 mM, 0.064 mM, and 0.0128 mM, while those for CB-839 were 2000 μM, 400 μM, 80 μM, 16 μM, 3.2 μM, 0.64 μM, 0.128 μM, and 0.0256 μM. After a duration of 5 days, the cells were harvested, and the final results were evaluated using a colorimetric assay.

Flow Cytometry

Both NUGC2 and MycER cell lines were cultured for 5 days under normal media conditions, in glutamine-deprived media, or in media supplemented with 7mM of alpha-ketoglutarate (aKG). After the 5-day period, 100,000 cells were trypsinized and then stained with Propidium Iodide Ready Flow™ Reagent, according to the manufacturer's instructions.

The staining process involved the following steps: Two drops of Propidium Iodide Ready Flow™ Reagent were added per 10^6 cells in 1 mL of suspension. Cells were then incubated for 15 minutes at room temperature (25°C). After incubation, the cells were analyzed by flow cytometry.

Flow cytometry was performed using the BD FACSARIA III Cell Sorter. The gating strategy adopted for cell sorting is illustrated in Supplementary Figures 3A-B. Detailed data analysis was carried out post-acquisition, using appropriate flow cytometry analysis software.

siRNA-mediated knockdown of Aldh4a1 and proliferation assay

Aldh18a1 select KD MycER MEFs were seeded in triplicate at 40,000 cells per well in 12 well plates using complete medium. The next day, an initial "day 0" seeding plate was trypsinized and counted as described above. The remaining plates were washed twice with PBS, medium replaced with glutamine -free DMEM, and cells transfected with ON-TARGETplus siRNAs purchased from Dharmacon targeting mouse *Aldh4a1* (#1: J-040250-09 ; #2 J-040250-10) or a non-targeting siRNA (d-001810-01) using Lipofectamine™ 2000 CD (Thermo Fisher Scientific) according to the standard protocol, using serum-free, glutamine -free DMEM instead of OPTI-MEM (which contains glutamine). The next day, medium was replaced with GLN-free DMEM to remove transfection reagent. Cells were trypsinized and counted each day for five days. On day three, cells were re-transfected with siRNAs, using the same protocol, in order to maintain

P5CDH knockdown. After counting, cells were pelleted and whole cell lysate extracted for western blot analysis of P5CDH expression.

LC-MS polar metabolomics

Intracellular metabolite extraction from adherent cells in culture: Cells were seeded in triplicate in 6-well plates (3 wells for metabolite extraction and 3 wells for protein quantification) using complete medium. When cells reached 70–80% confluence, metabolites were extracted and protein measured. When heavy isotope labeling was performed, medium was replaced 24 hours before extraction with DMEM with or without glutamine, supplemented with 10% dialyzed serum and 0.8mM $^{15}NH_4Cl$ (Millipore Sigma), as previously described (6). To extract metabolites, cells were washed twice with ice cold 0.9% NaCl. Cells were then extracted on dry ice in 1mL 80% methanol containing 500 nM internal standards (Metabolomics Amino Acid Mix Standard: Cambridge Isotope Laboratories). Cell extracts were collected using a cell scraper and transferred to a microcentrifuge tube. Samples were vortexed for 10min at 4°C and centrifuged at 17,000xg for 10min at 4°C. The supernatant was then transferred to a new microcentrifuge tube and evaporated using a speed-vac. Dried polar extracts were stored at −80°C until LC/MS analysis. Protein was determined by Bradford assay.

Intracellular metabolite extraction and LC/MS analysis of CRISPR KO Cells: Cells were grown in triplicate in 6-well plates for 24 hours in proline-free high-glucose DMEM medium with 0.65mM L-glutamine and 2.5% FBS. Then, metabolites were extracted and detected via LC-MS. Metabolite extraction and metabolomics was performed as described in Mackay et al. (45). The data analysis was performed with the TraceFinder software (Thermo Fisher Scientific) and peak areas normalized to protein quantity measured by the Lowry protein assay.

Targeted Polar Metabolomics Analysis Using LC-MS in Extended Data Fig. 2B: Polar metabolites were extracted from MycER shScram and sh*Aldh18a1* #2 cells, following 24 hours incubation in glutamine-free medium, and were subjected to liquid chromatography-mass spectrometry (LC-MS) analysis using an ID-X system. A stock solution of canonical amino acid mix from Cambridge Isotope (MSK-CAA-1) was prepared according to the manufacturer's instructions and was used as an internal standard. Metabolites were extracted from the cells using 100% methanol. The extracted samples were then centrifuged to remove any particulate matter. The supernatant was collected and dried using a speed vacuum concentrator. The dried samples were re-suspended in 70% acetonitrile, and d8-valine was added as an additional internal standard for resuspension. Analysis was carried out using a Zic-pHILIC column (150×2.1mm, 5μm) with a binary gradient system of 20 mM ammonium carbonate and 0.1% ammonium hydroxide in water (A), and 97% acetonitrile in water (B). The injection volume was 5 μL. The gradient program was as follows (time in min, % of phase B): 0 min, 93%, 0.5 min, 93%, 19 min, 40%, 28 min, 0%, 33 min, 0%, 36 min, 93%, 45 min, 93%. The flow rate was maintained at 0.15 mL/min after an initial 0.5 min at 0.05 mL/min. The mass spectrometer was operated in both positive (HESI+) and negative (HESI-) ionization modes. The MS parameters were as follows for both polarities: Resolution - 240,000; RF lens - 30%; Normalized AGC target - 25%; Maximum injection

time (IT) - 50 ms; m/z range: 65 to 1000. Internal calibration was performed according to the manufacturer's guidelines. The acquired data was processed using the Xcalibur software suite and the Quant Browser tool for peak identification, integration, and metabolite quantification. The concentrations of metabolites were calculated by comparing their peak areas to those of the internal standards.

For untargeted metabolomics with Stable Isotope Labeling in Fig. 2C, 3D, Extended Data Fig. 4B, Fig. 5D and Extended Data Fig. 7B: we employed isotopically labeled metabolites for tracing experiments. Specifically, we used ^{13}C5-glutamine (Cambridge Isotope, CLM-1822-H-0.25) and ^{13}C5-glutamate (Cambridge Isotope, CLM-1800-H-0.25). Cells were starved in glutamine-free media with 10% dialyzed FBS for 24 hours prior to the experiment. Subsequently, cells were incubated with glutamine-free media with 10% dialyzed FBS containing 500 μM of ^{13}C5-glutamine or respectively 5 mM ^{13}C5-glutamate for an additional 24 hours. The sample preparation procedure was identical to the one described in the targeted polar metabolomics analysis section. LC-MS analysis was performed under the same conditions as described in the targeted metabolomics analysis. The acquired data was processed using Compound Discoverer 3.2 software (Thermo Fisher Scientific). This software was utilized for peak detection, alignment, and identification. Furthermore, it was employed for metabolite identification and quantification, and for tracing the incorporation of the ^{13}C-label into various metabolites.

Absolute quantification of glutamine, glutamate, and proline in the media (Extended Data Fig. 1E): same conditions as described above were utilized, with the incorporation of a standard curve for absolute quantification. The standard curve was prepared with the following concentrations: 1000 μM, 200 μM, 40 μM, 8 μM, 0.32 μM, 0.064 μM, 0.001 μM, and 0 μM of glutamine, glutamate and proline and a mix of labeled AAs were added for internal standard (MSK-CAA-1). The absolute quantification was computed utilizing Xcalibur Quant Browser software.

Data analysis: statistical significance was assessed using two-way analysis of variance (ANOVA). The results were considered statistically significant when the p-value was less than 0.05. All statistical tests were performed using GraphPad Prism 9.5 software

GC/MS analysis for GLN/Pro stable isotope labeling experiment

MycER MEFs were seeded in a 6-well plate (300,000 cells per well) in complete medium. The next day, cells were washed 2x w/ PBS, the medium was removed and replaced with DMEM supplemented with 10% dialyzed FBS (GIBCO) and 1% penicillin-streptomycin (10,000 U/mL) (Gibco), 2mM of Arginine, 2mM Proline, 2mM ornithine, and 2mM of labeled Glutamine (13C5) (Cambridge Isotope Laboratories Inc.). 24 hours later the cells were harvested for gas chromatography-mass spectrometry (GC-MS).

Metabolite levels and isotopic forms were assessed using gas chromatography-mass spectrometry (GC-MS) according to established procedures (46). In summary, cells were rapidly frozen in liquid nitrogen. A dual-phase extraction process employing methanol and chloroform was used for metabolite extraction, followed by phase separation at 4°C. The polar extract was obtained, evaporated using a SpeedVac, and stored at −80°C.

Derivatization was performed first with methoxyamine (20 mg/ml in pyridine) for 90 minutes at 37°C, followed by N-(tert-butyldimethylsilyl)-N-methyl-trifluoroacetamide for one hour at 60°C. A 7890A GC system (Agilent Technologies) was utilized for measuring metabolite concentrations and isotopic patterns. Matlab with Metran software were used for data extraction from the raw ion chromatograms, and isotopomers were quantified as a proportion of the total amount as previously described (46).

Xenograft studies

For subcutaneous xenografts, MKN45 or EN cancer cells were first pre-conditioned by long-term culture (~3 weeks) in complete or GLN deprived media. 1×10^6 (MKN45) or 2×10^6 (EN) cells complete and GLN deprived conditions) suspended in 100µl PBS + 20% matrigel (Corning, 354234) were injected subcutaneously into matching lower flanks of male (MKN45) or female (EN) NOD SCID mice (Jackson Laboratories, 001303, 8 weeks old; gift from Nabeel Bardeesy, MGH Center for Cancer Research). Tumor size was measured every 7 days using a digital caliper, until the protocol-approved size limit was reached (15mm).

For subcutaneous xenografts of Human gastric cancer NUGC2 cells. The cell lines were cultured in appropriate growth medium supplemented with 10% fetal bovine serum (FBS) and 1% penicillin-streptomycin at 37°C in a humidified atmosphere containing 5% CO2. Three conditions were established: control NUGC2 cells transduced with PLKO (Control) and inducible RFP (pCW57-RFP-P2A-MCS), NUGC2 cells with shRNA-mediated knockdown of *ALDH18A1* (sh*ALDH18A1*) and inducible RFP expression (pCW57-RFP-P2A-MCS), and rescue NUGC2 cells with sh*ALDH18A1* and inducible *ALDH18A1* (pCW57-RFP-*ALDH18A1*-P2A-MCS) expression (Rescue). The knockdown of *ALDH18A1* was achieved by targeting the 5' untranslated region (UTR) using a lentiviral shRNA system. Six-week-old male NOD-SCID mice were used for the subcutaneous xenograft experiments. Mice were maintained under specific pathogen-free conditions, and all animal experiments were performed in compliance with institutional guidelines and approved by the Institutional Animal Care and Use Committee. Mice were randomly assigned to one of the three experimental groups (Control, KD, or Rescue), with 8 mice per group. For the inoculation, 1 × 10^6 NUGC2 cells from each condition were suspended in a 50:50 mixture of phosphate-buffered saline (PBS) and Matrigel (BD Biosciences), and a total volume of 100 µL was subcutaneously injected into the right flank of each mouse.

Tumor Volume Measurements and Endpoint Criteria—Tumor growth was monitored, and tumor volumes were measured twice per week using digital calipers. Tumor volume was calculated using the following formula:

$$\text{Tumor volume } \left(\text{mm}^3\right) = \left(\text{length} \times \text{width}^2\right)/2$$

Statistical Analysis: mice were euthanized once their tumors reached a volume of 1500 mm^3 or at the end of the study, whichever occurred first. Tumors were harvested, weighed, and processed for further analyses. Data are presented as mean ± standard error of the mean (SEM). Comparisons between groups for tumor volumes were performed using

two-way ANOVA followed by post-hoc Tukey's multiple comparisons test. For other comparisons, one-way ANOVA followed by post-hoc Tukey's multiple comparisons test was used. Statistical analyses were conducted using GraphPad Prism, and a p-value < 0.05 was considered statistically significant. Data collection and analysis were not performed blind to the conditions of the experiments. Mice were housed under standard conditions in a controlled environment with a 12-hour light/dark cycle, temperature of 22±2°C, and 50±10% relative humidity. Animals had ad libitum access to water and were fed with Prolab Isopro RMH 3000 irradiated diet.

All xenograft experiments were approved by the MGH Institutional Animal Care and Use Committee (IACUC) under protocol number 2019N000111. No statistical methods were used to pre-determine sample sizes but our sample sizes are similar to those reported in previous publications (48).

Human Patients' Histology and immunostaining

Patient tissue blocks were selected from the tissue repository at the MGH Pathology Department and paraffin embedded tissues were sectioned to 5μm thickness. Patients provided written informed consent for use of their samples through the IRB protocol #2022P003117. The following primary antibodies were used: anti-P5CS (Novus Biologicals, NBP1-88324) 1:100, anti-GS (Millipore Sigma, MAB302) 1:8,000. Counterstaining was performed with hematoxylin. Slides were scanned and imaged at 20x and 40x magnification using Aperio Scanscope XT (Leica Biosystems). Image analysis was performed on Halo 3.1 (Indica Labs) using the Multiplex IHC v2.3.4 algorithm. Optical density was determined for hematoxylin and DAB for each marker. For region analysis in multiple slides we used the Halo Image Registration processing tool, which aligns adjacent tissue sections. All areas analyzed were user drawn and cells counted including their optical density for DAB in P5CS and GS-stained slides. Data is presented as average optical density for each marker.

Statistical analysis

For proliferation assays, crystal violet quantifications, western blot quantifications, polar metabolomics data, and tumor size, statistical significance was determined using Student's t-tests. A p-value less than 0.05 was considered statistically significant. Statistics were performed using GraphPad Prism.

Data distribution was assumed to be normal but this was not formally tested.

Extended Data

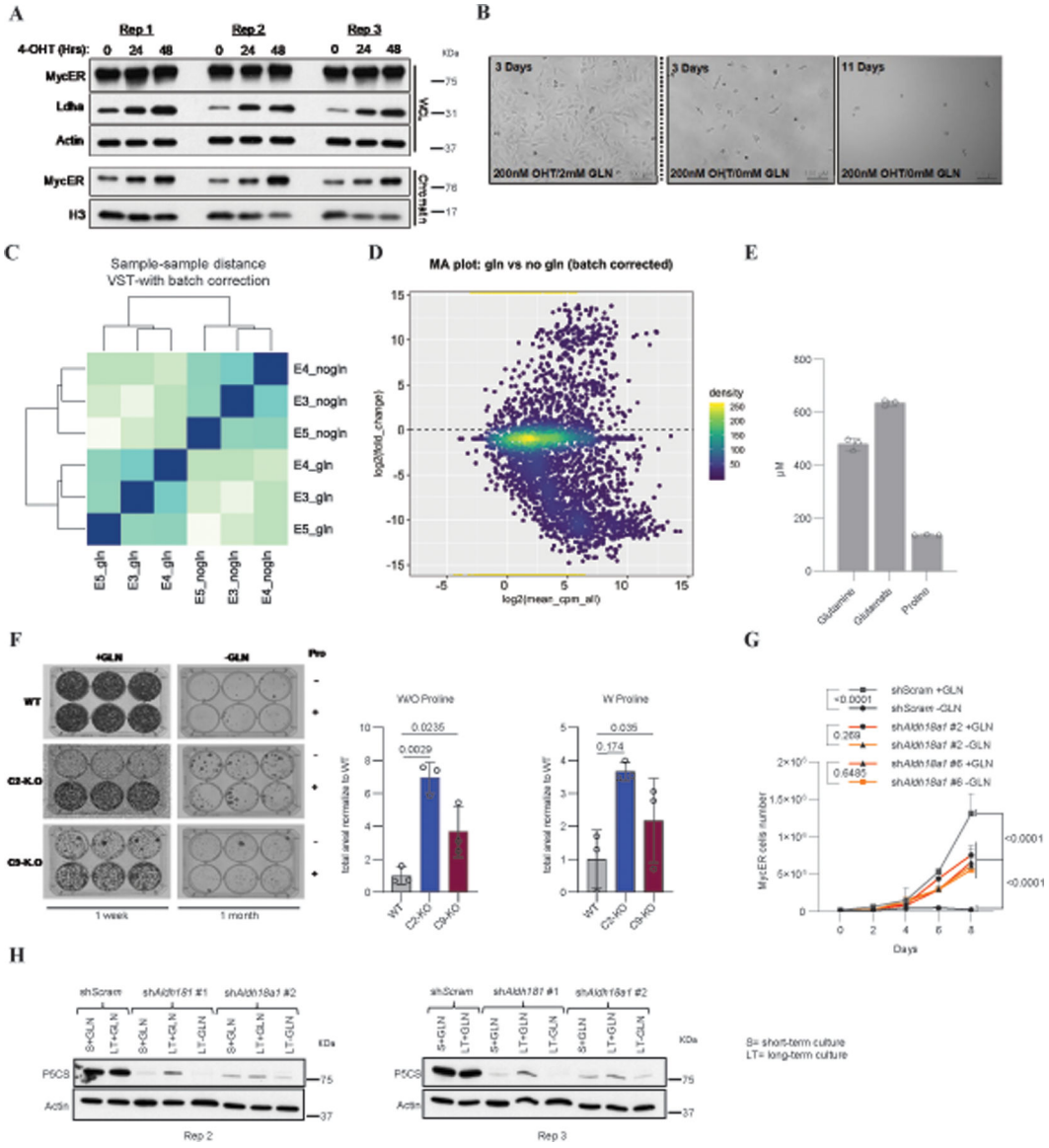

Extended Data Figure 1. Quality controls of the genome-wide shRNA-library, GLN deprivation screen.

A) Western blot of MycER and Myc transcriptional target Ldha in whole cell lysate (WCL) and chromatin isolated from MycER MEFs exposed to 200nM 4-OHT for 24 and 48 hours. **B)** Phase contrast microscopy of MycER cells + 200nM 4-OHT grown in normal media for 3 days or without GLN for 3 and 11 days. **C)** Heatmap showing pairwise sample-sample Euclidean distances, arranged by treatment group. Dendrograms show hierarchical clustering to highlight similarities between samples. **D)** MA plot of $\log_2$(mean counts-per-million) against $\log_2$(median fold-change), with points colored by density to highlight data trend(s). **E**) Levels of Glutamine (GLN), Glutamate (GLU), and Proline (PRO) in Fetal bovine serum. Data are represented as mean ± SD of three independent experiments **F**) WT and two clonal P5CS CRISPR KO mouse kidney epithelial cell lines grown in the

presence of 2mM GLN for 1 week, or absence of GLN for 1 month, with corresponding quantification of growth. Statistically significant differences were evaluated using a paired, one-tailed T-Test, with the error bars representing standard deviation (SD). **G**) Growth curves of control and Aldh18a1 knockdown cells under +GLN and -GLN conditions. Data are represented as mean ± SD of three independent experiments. Statistical significance was determined using two-way ANOVA. **H**) Repeats of western blot against P5CS in short-term (S) or long-term (L) culture of shScram and shAldh18a1 MycER MEFs in the presence or absence of 2mM glutamine. * $p \leq 0.05$, ** $p \leq 0.01$, *** $p \leq 0.01$, **** $p \leq 0.0001$.

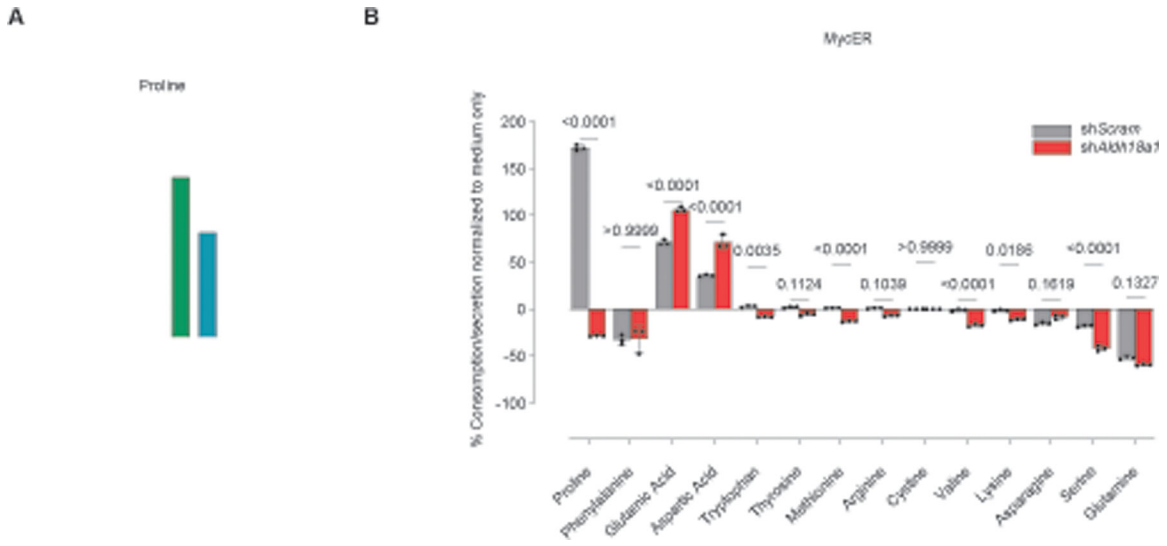

Extended Data Figure 2. Proline depletion upon P5CS/*Aldh18a1* downregulation.

A) Relative abundance of intracellular PRO in WT mouse kidney epithelial cells from two different thaws (WT-1 and WT-2) and two P5CS KO subclones (C2 and C9) infected either with empty vector (+Vec) or reconstituted with P5CS (+P5CS). Cells were grown for 24 hours in proline-free high-glucose DMEM medium with 0.65mM GLN and 2.5%FBS, and metabolite levels normalized by total protein (n=3) Statistical significance was determined using an unpaired, T-Test, with error bars indicating SD. **B**) Metabolomic profiling of amino acid consumption and secretion. This panel of plots illustrates the relative consumption and secretion rates of various amino acids by control and P5CS KD cells, under low-glutamine conditions. The lower bar graphs show the consumption rates of amino acids from the media, while the upper ones depict the secretion rates of amino acids into the media. Data are represented as mean ± SD of three independent experiments. The statistical analysis was performed using two-way ANOVA. * $p \leq 0.05$, ** $p \leq 0.01$, *** $p \leq 0.01$, **** $p \leq 0.0001$.

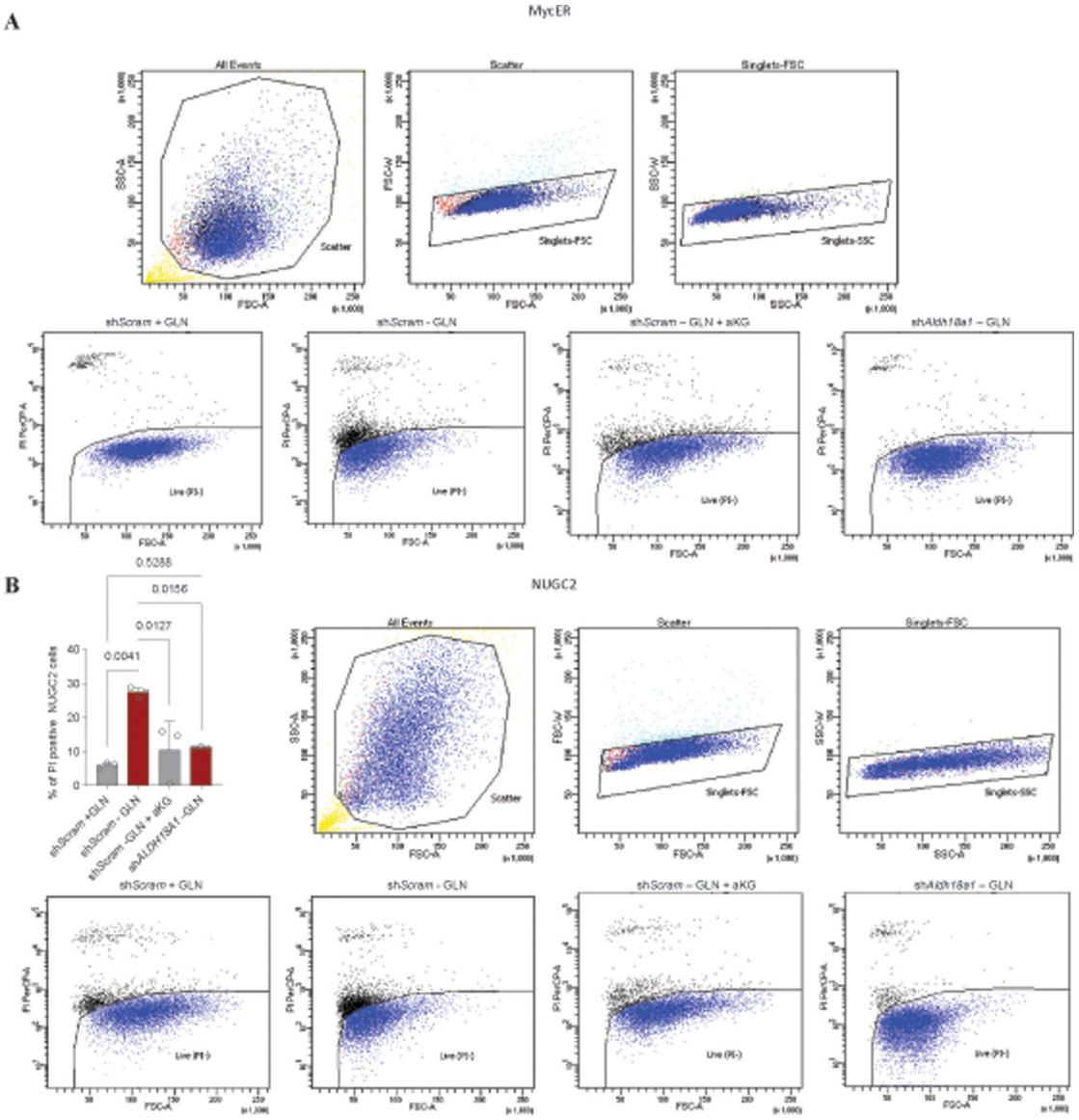

Extended Data Figure 3. Evaluation of Cell Death in Response to Glutamine Deprivation

A) Gating strategy for sorting MycER control cells and shALDH18A1 cells under different conditions: normal medium, glutamine-deprived medium, and medium supplemented with 7 mM alpha-ketoglutarate (aKG). **B**) Propidium iodide staining of NUGC2 control and shALDH18A1 cells quantified by Flow cytometry. Data are presented as mean ± SD from three independent experiments. Statistical analysis was performed using two-way ANOVA. On the right, the gating strategy for sorting in control and shALDH18A1 NUGC2 cells under different conditions: normal medium, glutamine-deprived medium, and medium supplemented with 7 mM alpha-ketoglutarate (aKG). * $p \leq 0.05$, ** $p \leq 0.01$, *** $p \leq 0.01$, **** $p \leq 0.0001$.

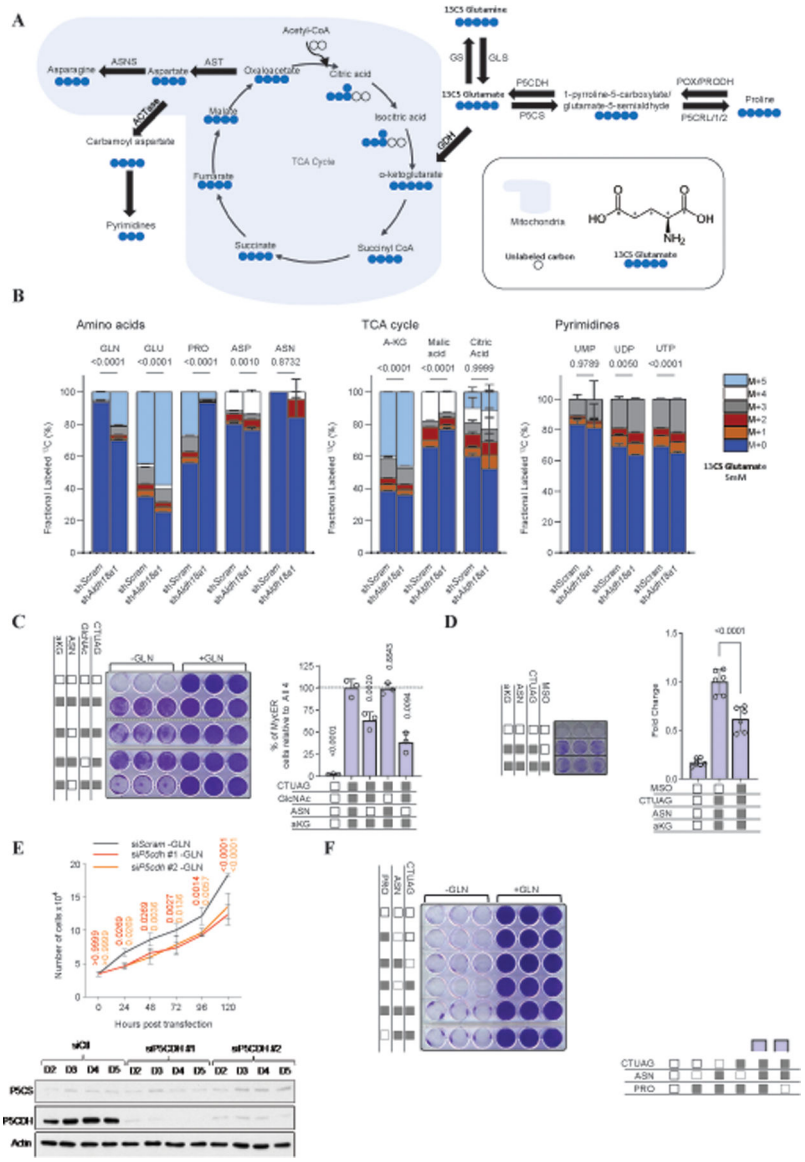

Extended Data Figure 4. Proline is not a major source of carbon and/or nitrogen in GLN-starved cells.

A) Graphical representation of the 13C5 glutamate labeling pathway, illustrating its incorporation into intermediates of the TCA cycle, amino acids, and pyrimidines. **B**) Tracer experiment using 13C5 labeled glutamate in Control and P5CS Knockdown Cells. The bar chart illustrates the proportion of proline derived from glutamine in both control and P5CS knockdown cells, as well as the corresponding increase in the labeling of amino acids, nucleosides, and TCA cycle intermediates. Data are represented as mean ± SD of three independent experiments. The statistical analysis was performed using two-way ANOVA. **C**) Crystal violet staining and corresponding quantification of MycER shScram cells cultured in the presence or absence of GLN for 5 days. Cells were cultured in DMEM supplemented with 7mM dimethyl-α-ketoglutarate (α-KG), 2mM ASN, 15mM GlcNAc, or 250μM each cytidine (C), thymidine (T), uridine (U), adenosine (A), and guanosine (G) in indicated combinations. Statistical significance was determined using an unpaired, Two-

tailed, T-Test, with error bars indicating SD. **D**) Crystal violet staining and corresponding quantification of MycER shScram cells cultured in the presence or absence of GLN for 5 days. Cells were cultured in DMEM supplemented with 7mM dimethyl-α-ketoglutarate (α-KG), 2mM ASN, 15mM GlcNAc, or 250μM each cytidine (C), thymidine (T), uridine (U), adenosine (A), and guanosine (G) in presence or absence of L-Methionine sulfoximine (MSO). Statistical significance was determined using ordinary one-way ANOVA followed by Tukey's post hoc test for multiple comparisons. Error bars represent standard deviation (SD). **E**) Cell proliferation of *Aldh18a1* KD cells transfected with either siScram or two independent siP5CDH grown in the absence of GLN for 5 days (n=3) (Top). Corresponding western blot verifying P5CS and P5CDH knockdown (Bottom). Statistical significance was determined using ordinary one-way ANOVA followed by Tukey's post hoc test for multiple comparisons. Error bars represent standard deviation (SD). **F**) Crystal violet staining and corresponding quantification of MycER shScram cells cultured in the presence or absence of GLN for 5 days. Cells were cultured in DMEM supplemented with 0.5mM Proline, 2mM ASN, or 250uM each C, T, U, A, and G, in indicated combinations. All error bars are SD. Grey square: Presence, white square: Absence * $p \leq 0.05$, ** $p \leq 0.01$, *** $p \leq 0.01$, **** $p \leq 0.0001$.

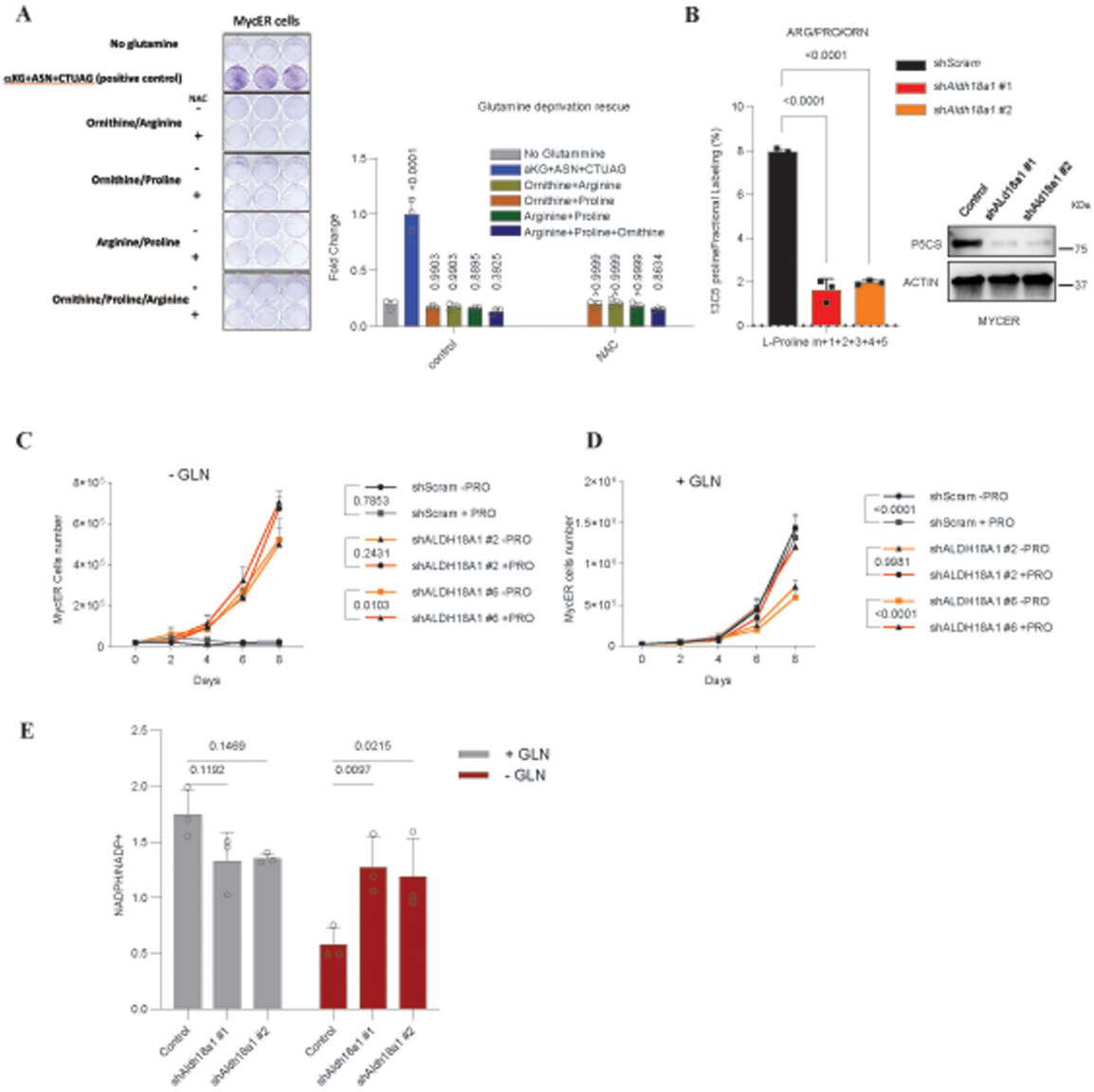

Extended Data Figure 5. Downregulation of P5CS maintains NADPH/ NADP+ ratio in low GLN

A) Crystal violet staining and corresponding quantification of MycER cells cultured in the absence of GLN or in the presence of aKG (7mM) + ASN (2mM) + C,T,U,A, and G (250uM each) or Ornithine/arginine 2mM or Ornithine/Proline 2mM or Arginine/Proline 2mM, or Ornithine/proline/Arginine 2mM. Each condition with or without N-Acetyl Cysteine (NAC) 5 days. Statistical significance was determined using ordinary one-way ANOVA followed by Dunnett's post hoc test for multiple comparisons. Error bars represent standard deviation (SD). **B**) This represents the percentage of incorporation of 13C5-labeled glutamine into L-Proline in MycER shScram, shAldh18a1 #1, and shAldh18a1 #2 cells. These cells were cultured in DMEM supplemented with dialyzed FBS and 2mM each of labeled Glutamine (13C5), Arginine, Proline, and Ornithine (n=3). The fraction that was not labeled was designated as Proline M+0. Corresponding western blot verifying P5CS knockdown (right side). Statistical significance was determined using ordinary one-way ANOVA followed by Dunnett's post hoc test for multiple comparisons. Error bars represent standard deviation

(SD). **C** and **D**) Left panel: Growth curves of control and Aldh18a1 knockdown cells under -GLN and +GLN conditions, in the presence of 0.5 mM Proline. Data are represented as mean ± SD of three independent experiments. Statistical significance was determined using a two-way ANOVA. Right panel: Growth curves of control and Aldh18a1 knockdown cells under +Proline and -Proline conditions, in the context of +GLN. Data are represented as mean ± SD of three independent experiments. The statistical analysis was performed using a two-way ANOVA. **E**) bar graph representing the NADPH/NADP+ ratio in MycER cells, comparing the control group with two separate shALDH18A1 knockdown groups, under low glutamine conditions for 48 hours. Data are represented as mean ± SD of three independent experiments. The statistical analysis was performed using two-way ANOVA. * $p \leq 0.05$, ** $p \leq 0.01$, *** $p \leq 0.01$, **** $p \leq 0.0001$.

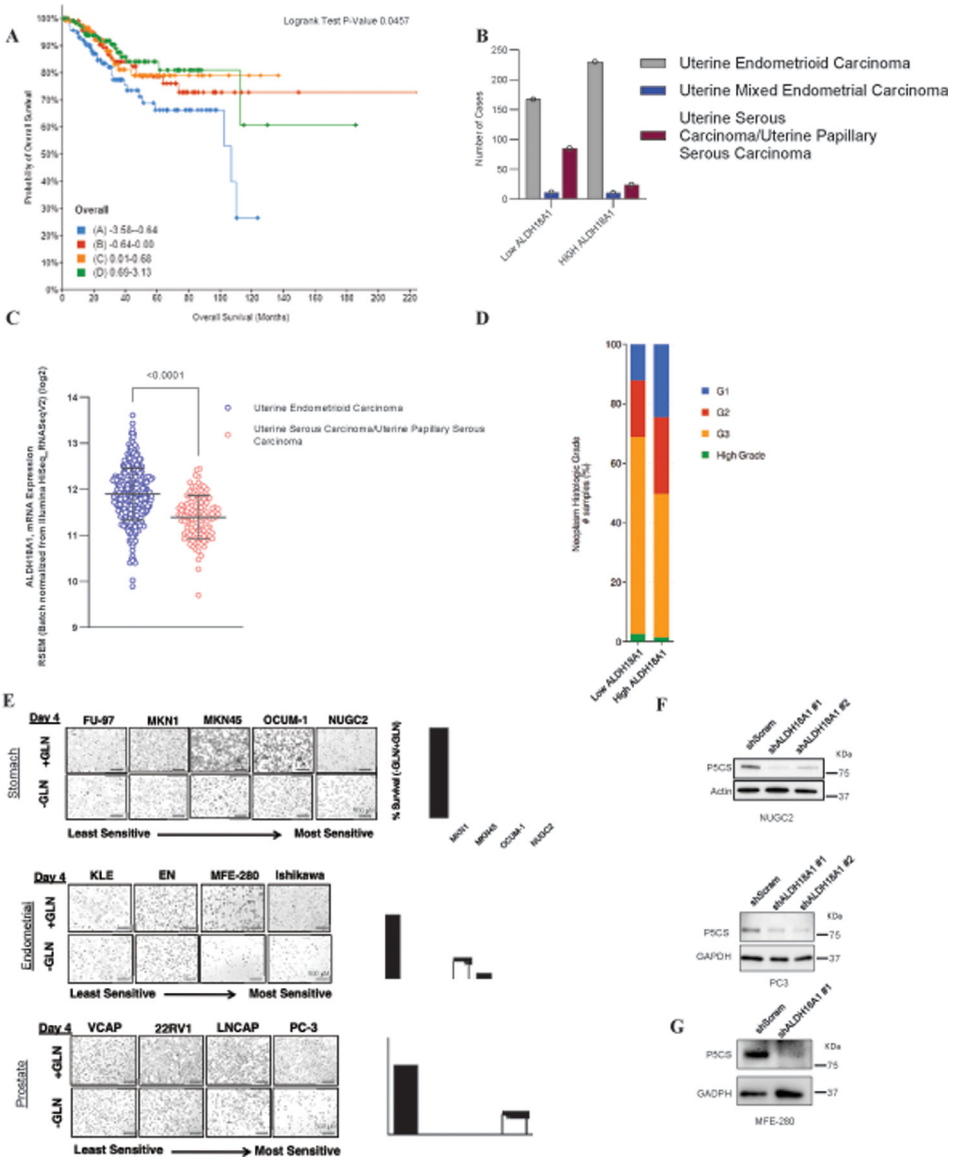

Extended Data Figure 6. Sensitivity of human cancer cell lines to GLN restriction.

A) Kaplan-Meier survival curves analyzing the The Cancer Genome Atlas (TCGA) human uterine/endometrial or stomach cancer patient samples based on Aldh18a1 mRNA expression divided in quartiles. **B)** Bar plot illustrating the distribution of Uterine Endometrioid Carcinoma, Uterine Mixed Endometrial Carcinoma, and Uterine Serous Carcinoma cases, classified by low or high expression levels of ALDH18A1. (TCGA) **C**) Scatter plot demonstrating the ALDH18A1 mRNA expression levels across Uterine Endometrioid Carcinoma and Uterine Serous Carcinoma cases, based on TCGA data. Statistical analysis was conducted using an unpaired two-tailed t-test, and data are presented as mean ± SD. **D**) Bar plot demonstrating the distribution of Uterine cancer cases by histological grade, categorized by low or high ALDH18A1 RNA expression, as per TCGA data. **E**) Representative images and quantification of sensitivity to glutamine depletion of human cancer cell lines grown in the presence or absence of GLN for 4 days, represented by percent survival. Survival was calculated by dividing the average number of cells counted on Day 4 in wells treated with no GLN by the average number of cells in wells with GLN (n = 3 wells). **F**) Western blot analysis of NUGC2 and PC3 cell lines using scramble shRNA or two independent shRNAs targeting the 3'UTR of ALDH18A1.

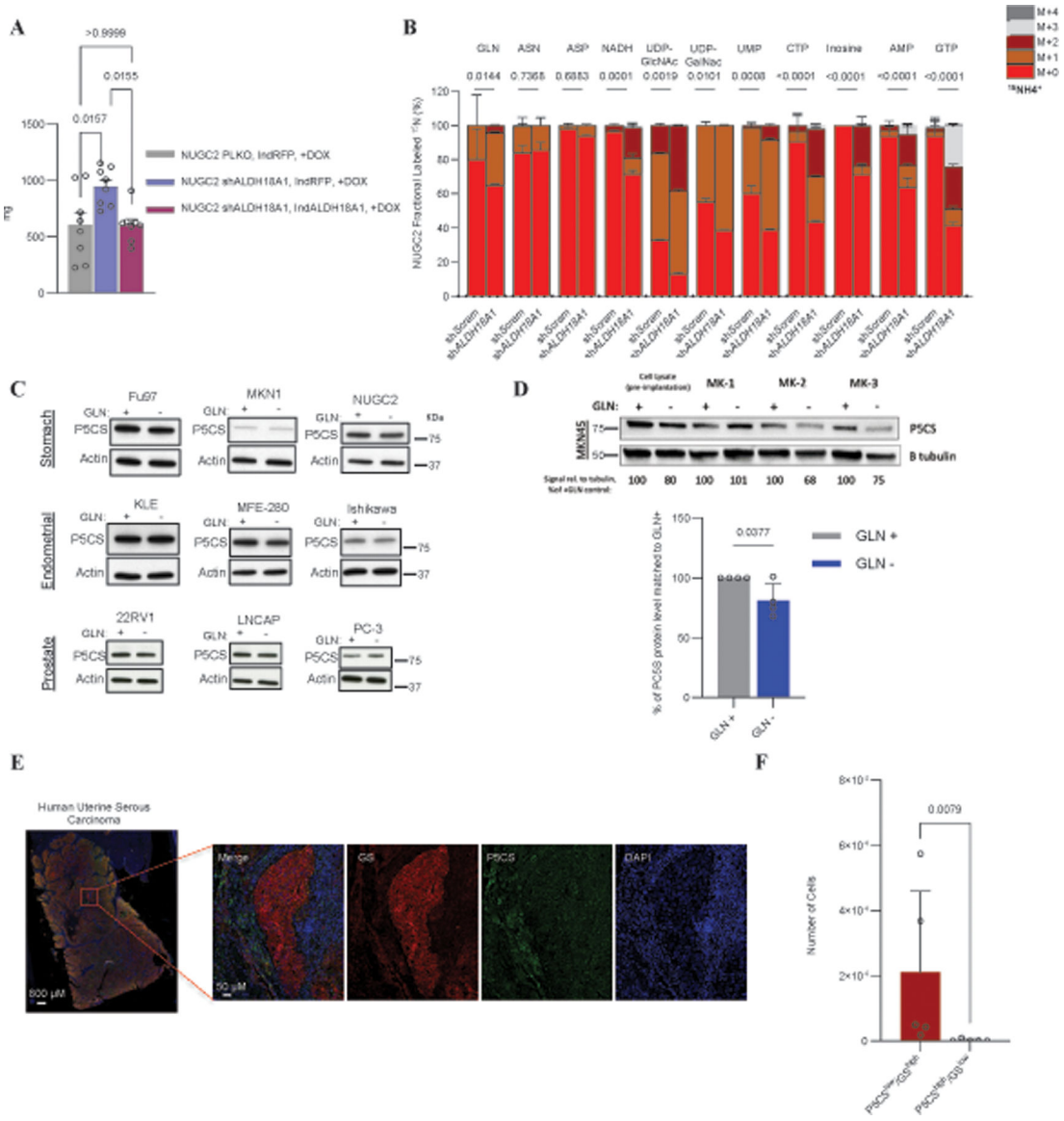

Extended Data Figure 7. Variation in P5CS Expression Levels among Human Cancer Cell Lines under Glutamine Deprivation

A) Bar plot illustrating the weights of subcutaneous xenograft tumors from NUGC2 cells (PLKO, shALDH18A1, and rescue with dox-inducible NUGC2). Statistical analysis was conducted using a one-way ANOVA followed by Tukey's multiple comparison test. Error bars represent standard deviation (SD). **B**) 15N-labeled ammonia (15NH4+) in NUGC2 gastric cancer cells with genetically downregulated P5CS. Data are represented as mean ± SD of three independent experiments. Statistical significance was determined using two-way ANOVA. **C)** Western blot of P5CS in human cancer cell lines that do not endogenously downregulate P5CS upon acute GLN starvation. Cells were cultured in the presence or absence of 2mM GLN for 24 hrs. **D**) Comparison of P5CS levels in xenograft tumors derived from MKN45 cells. On the left, a western blot illustrates the relative P5CS protein levels in tumor extracts, while on the right, a bar graph represents the quantification of these levels. Statistical significance was determined using a one-tailed unpaired t-test with

Welch's correction for unequal variances, with error bars indicating standard deviation (SD). **E**) Additional representative immunofluorescence (IF) of a tumor section of uterine serous carcinoma, depicting staining by IF for P5CS (red), GS (green), and Dapi (blue). On the right, a selected area of the tumors demonstrates an inverse correlation between P5CS and GS expression. **F**) Total number of cells with partner $P5CS^{low}/GS^{high}$ or vice-versa detected in five tumor sections of uterine serous carcinoma (USC). Statistical analysis was performed using an unpaired two-tailed Mann-Whitney test, and the standard deviation (SD) is shown. $p \leq 0.05$, ** $p \leq 0.01$, *** $p \leq 0.01$, **** $p \leq 0.0001$.

Supplementary Material

Refer to Web version on PubMed Central for supplementary material.

Acknowledgments:

We would like to thank all members of the Mostoslavsky lab for helpful discussions and critical reading of the manuscript. We thank Ralph DeBerardinis (University of Texas Southwestern Medical Center) for providing the MycER MEF cell line used in the screen, and the Metabolite Profiling Core (Whitehead Institute) for their helpful discussions and technical expertise. S.J.L. is the recipient of an NIH F31 Ruth L. Kirschstein Predoctoral fellowship (F31CA210310);T. B. is recipient of an EMBO post-doctoral Fellowship; R. Mostoslavsky is the Laurel Schwartz Endowed Chair in Oncology. This work is partially supported by NIH grants R33ES025638 and R01GM128448 and a Massachusetts Life Sciences Center (MLSC) Bits to Bytes award to R. Mostoslavsky, NIH grants R01CA117907, R01GM120109, and P30CA046934, NSF grant MCB-1817582, and grants from the Wings of Hope and Golfers Against Cancer foundations to J.M.E. B.R.R. is funded by the Nile Albright Research Foundation and Vincent Memorial Hospital Foundation.

Data availability:

The Datasets for the shRNA screening has been deposited in the NCBI Gene Expression Omnibus (GEO), Accession Number GSE162314. Other data have been provided as source data with the article or will be available upon request.

REFERENCES:

1. Altman ABJ, Stine ZE, Dang CV, From Krebs to clinic: glutamine metabolism to cancer therapy. Nat Rev Cancer. 16, 619–34 (2016). [PubMed: 27492215]
2. Zhang J, Pavlova NN, Thompson CB, Cancer cell metabolism: the essential role of the nonessential amino acid, glutamine. Embo J 36, 1302–1315 (2017). [PubMed: 28420743]
3. Krebs HA, Metabolism of amino-acids: The synthesis of glutamine from glutamic acid and ammonia, and the enzymic hydrolysis of glutamine in animal tissues. Biochem J 29, 1951–69 (1935). [PubMed: 16745865]
4. Eagle H, The minimum vitamin requirements of the L and HeLa cells in tissue culture, the production of specific vitamin deficiencies, and their cure. J Exp Medicine. 102, 595–600 (1955).
5. Bott J, Peng I-C, Fan Y, Faubert B, Zhao L, Li J, Neidler S, Sun Y, Jaber N, Krokowski D, Lu W, Pan J-A, Powers S, Rabinowitz J, Hatzoglou M, Murphy DJ, Jones R, Wu S, Girnun G, Zong W-X, Oncogenic Myc Induces Expression of Glutamine Synthetase through Promoter Demethylation. Cell Metab 22, 1068–77 (2015). [PubMed: 26603296]
6. Tardito S, Oudin A, Ahmed SU, Fack F, Keunen O, Zheng L, Miletic H, Sakariassen PØ, Weinstock A, Wagner A, Lindsay SL, Hock AK, Barnett SC, Ruppin E, Mørkve SH, Lund-Johansen M, Chalmers AJ, Bjerkvig R, Niclou SP, Gottlieb E, Glutamine synthetase activity fuels nucleotide biosynthesis and supports growth of glutamine-restricted glioblastoma. Nat Cell Biol 17, 1556–68 (2015). [PubMed: 26595383]

7. Pavlova NN, Hui S, Ghergurovich JM, Fan J, Intlekofer AM, White RM, Rabinowitz JD, Thompson CB, Zhang J, As Extracellular Glutamine Levels Decline, Asparagine Becomes an Essential Amino Acid. Cell Metab 27, 428–438.e5 (2018). [PubMed: 29337136]
8. Bott J, Shen J, Tonelli C, Zhan L, Sivaram N, Jiang Y-P, Yu X, Bhatt V, Chiles E, Zhong H, Maimouni S, Dai W, Velasquez S, Pan J-A, Muthalagu N, Morton J, Anthony TG, Feng H, Lamers WH, Murphy DJ, Guo JY, Jin J, Crawford HC, Zhang L, White E, Lin RZ, Su X, Tuveson DA, Zong W-X, Glutamine Anabolism Plays a Critical Role in Pancreatic Cancer by Coupling Carbon and Nitrogen Metabolism. Cell Reports. 29, 1287–1298.e6 (2019). [PubMed: 31665640]
9. Wise DR, DeBerardinis RJ, Mancuso A, Sayed N, Zhang X-Y, Pfeiffer HK, Nissim I, Daikhin E, Yudkoff M, McMahon SB, Thompson CB, Myc regulates a transcriptional program that stimulates mitochondrial glutaminolysis and leads to glutamine addiction. P Natl Acad Sci Usa 105, 18782–7 (2008).
10. Mayers JR, Heiden MGV, Famine versus feast: understanding the metabolism of tumors in vivo. Trends Biochem Sci 40, 130–40 (2015). [PubMed: 25639751]
11. Roberts E, Simonsen DG, Tanaka KK, Tanaka T, Free amino acids in growing and regressing ascites cell tumors: host resistance and chemical agents. Cancer Res 16, 970–8 (1956). [PubMed: 13374707]
12. Rivera S, Azcón-Bieto J, López-Soriano FJ, Miralpeix M, Argilés JM, Amino acid metabolism in tumour-bearing mice. Biochem J 249, 443–449 (1988). [PubMed: 3342022]
13. Márquez J, Sánchez-Jiménez F, Medina MA, Quesada AR, de Castro IN, Nitrogen metabolism in tumor bearing mice. Arch Biochem Biophys 268, 667–675 (1989). [PubMed: 2913952]
14. Pan M, Reid MA, Lowman XH, Kulkarni RP, Tran TQ, Liu X, Yang Y, Hernandez-Davies JE, Rosales KK, Li H, Hugo W, Song C, Xu X, Schones DE, Ann DK, Gradinaru V, Lo RS, Locasale JW, Kong M, Regional glutamine deficiency in tumours promotes dedifferentiation through inhibition of histone demethylation. Nat Cell Biol 18, 1090–1101 (2016). [PubMed: 27617932]
15. Lee S-W, Zhang Y, Jung M, Cruz N, Alas B, Commisso C, EGFR-Pak Signaling Selectively Regulates Glutamine Deprivation-Induced Macropinocytosis. Dev Cell 50, 381–392.e5 (2019). [PubMed: 31257175]
16. Yuneva M, Zamboni N, Oefner P, Sachidanandam R, Lazebnik Y, Deficiency in glutamine but not glucose induces MYC-dependent apoptosis in human cells. J Cell Biology 178, 93–105 (2007).
17. Zhang J, Fan J, Venneti S, Cross JR, Takagi T, Bhinder B, Djaballah H, Kanai M, Cheng EH, Judkins AR, Pawel B, Baggs J, Cherry S, Rabinowitz JD, Thompson CB, Asparagine plays a critical role in regulating cellular adaptation to glutamine depletion. Mol Cell 56, 205–18 (2014). [PubMed: 25242145]
18. Krall S, Xu S, Graeber TG, Braas D, Christofk HR, Asparagine promotes cancer cell proliferation through use as an amino acid exchange factor. Nat Commun 7, 11457 (2016). [PubMed: 27126896]
19. Yang L, Achreja A, Yeung T-L, Mangala LS, Jiang D, Han C, Baddour J, Marini JC, Ni J, Nakahara R, Wahlig S, Chiba L, Kim SH, Morse J, Pradeep S, Nagaraja AS, Haemmerle M, Kyunghee N, Derichsweiler M, Plackemeier T, Mercado-Uribe I, Lopez-Berestein G, Moss T, Ram PT, Liu J, Lu X, Mok SC, Sood AK, Nagrath D, Targeting Stromal Glutamine Synthetase in Tumors Disrupts Tumor Microenvironment-Regulated Cancer Cell Growth. Cell Metab 24, 685–700 (2016). [PubMed: 27829138]
20. Linares JF, Cordes T, Duran A, Reina-Campos M, Valencia T, Ahn CS, Castilla EA, Moscat J, Metallo CM, Diaz-Meco MT, ATF4-Induced Metabolic Reprograming Is a Synthetic Vulnerability of the p62-Deficient Tumor Stroma. Cell Metab 26, 817–829.e6 (2017). [PubMed: 28988820]
21. Mishra R, Haldar S, Placencio V, Madhav A, Rohena-Rivera K, Agarwal P, Duong F, Angara B, Tripathi M, Liu Z, Gottlieb RA, Wagner S, Posadas EM, Bhowmick NA, Stromal epigenetic alterations drive metabolic and neuroendocrine prostate cancer reprogramming. J Clin Invest 128, 4472–4484 (2018). [PubMed: 30047926]
22. Tajan M, Hock AK, Blagih J, Robertson NA, Labuschagne CF, Kruiswijk F, Humpton TJ, Adams PD, Vousden KH, A Role for p53 in the Adaptation to Glutamine Starvation through the Expression of SLC1A3. Cell Metab 28, 721–736.e6 (2018). [PubMed: 30122553]

23. Alkan HF, Walter KE, Luengo A, Madreiter-Sokolowski CT, Stryeck S, Lau AN, Al-Zoughbi W, Lewis CA, Thomas CJ, Hoefler G, Graier WF, Madl T, Heiden MGV, Bogner-Strauss JG, Cytosolic Aspartate Availability Determines Cell Survival When Glutamine Is Limiting. Cell Metab 28, 706–720.e6 (2018). [PubMed: 30122555]
24. Lowman XH, Hanse EA, Yang Y, Gabra MBI, Tran TQ, Li H, Kong M, p53 Promotes Cancer Cell Adaptation to Glutamine Deprivation by Upregulating Slc7a3 to Increase Arginine Uptake. Cell Reports 26, 3051–3060.e4 (2019). [PubMed: 30865893]
25. Jiang J, Srivastava S, Zhang J, Starve Cancer Cells of Glutamine: Break the Spell or Make a Hungry Monster? Cancers. 11, 804 (2019). [PubMed: 31212591]
26. Hu CA, Lin WW, Obie C, Valle D, Molecular enzymology of mammalian Delta1-pyrroline-5-carboxylate synthase. Alternative splice donor utilization generates isoforms with different sensitivity to ornithine inhibition. J Biological Chem 274, 6754–62 (1999).
27. Olivares O, Mayers JR, Gouirand V, Torrence ME, Gicquel T, Borge L, Lac S, Roques J, Lavaut M-N, Berthezène P, Rubis M, Secq V, Garcia S, Moutardier V, Lombardo D, Iovanna JL, Tomasini R, Guillaumond F, Heiden MGV, Vasseur S, Collagen-derived proline promotes pancreatic ductal adenocarcinoma cell survival under nutrient limited conditions. Nat Commun 8, 16031 (2017). [PubMed: 28685754]
28. Zhu J, Schworer S, Berisa M, Kyung YJ, Ryu KW, Yi J, Jiang X, Cross JR, Thompson CB. Mitochondrial NADP(H) generation is essential for proline biosynthesis. Science 372, 968–972 (2021). [PubMed: 33888598]
29. Tran DH, Kesavan R, Rion H, Soflaee MH, Solmonson A, Bezwada D, Vu HS, Cai F, Phillips III JA, DeBerardinis RJ, Hoxhaj G. Mitochondrial NADP+ is essential for proline biosynthesis during cell growth. Nat. Metab 3, 571–585 (2021). [PubMed: 33833463]
30. Windmueller HG and Spaeth AE. Uptake and metabolism of plasma glutamine by the small intestine. J. Biol. Chem 249, 5070–5070 (1974). [PubMed: 4605420]
31. Liu W, Hancock C, Lane AN, Dang CV, Fan TW, Phang JM. Reprogramming of proline and glutamine metabolism contributes to the proliferative and metabolic responses regulated by oncogenic transcription factor c-MYC. Proc. Natl. Acad. Sci 109, 8983–8988 (2012). [PubMed: 22615405]
32. Liu W, Hancock CN, Fischer JW, Harman M, Phang JM, Proline biosynthesis augments tumor cell growth and aerobic glycolysis: involvement of pyridine nucleotides. Sci Rep-uk 5, 17206 (2015).
33. Burke L, Guterman I, Gallego RP, Britton RG, Burschowsky D, Tufarelli C, Rufini A, The Janus-like role of proline metabolism in cancer. Cell Death Discov 6, 104 (2020). [PubMed: 33083024]
34. Kardos GR, Wastyk HC, Robertson GP, Disruption of Proline Synthesis in Melanoma Inhibits Protein Production Mediated by the GCN2 Pathway. Mol Cancer Res 13, 1408–1420 (2015). [PubMed: 26082174]
35. Loayza-Puch F, Rooijers K, Buil LCM, Zijlstra J, Vrielink JFO, Lopes R, Ugalde AP, van Breugel P, Hofland I, Wesseling J, van Tellingen O, Bex A, Agami R, Tumour-specific proline vulnerability uncovered by differential ribosome codon reading. Nature. 530, 490–4 (2016). [PubMed: 26878238]
36. Sahu N, Dela Cruz D, Gao M, Sandoval W, Haverty PM, Liu J, Stephan J-P, Haley B, Classon M, Hatzivassiliou G, Settleman J, Proline Starvation Induces Unresolved ER Stress and Hinders mTORC1-Dependent Tumorigenesis. Cell Metab 24, 753–761 (2016). [PubMed: 27618686]
37. Sullivan KD, Lewis HC, Hill AA, Pandey A, Jackson LP, Cabral JM, Smith KP, Liggett LA, Gomez EB, Galbraith MD, DeGregori J, Espinosa JM, Trisomy 21 consistently activates the interferon response. Elife. 5, e16220 (2016). [PubMed: 27472900]
38. Langmead B, Salzberg SL, Fast gapped-read alignment with Bowtie 2. Nat Methods. 9, 357–9 (2012). [PubMed: 22388286]
39. Rubin H Deprivation of glutamine in cell culture reveals its potential for treating cancer. Proc Natl Acad Sci U S A 116, 6964–6968 (2019). [PubMed: 30877243]
40. Mathew R, Degenhardt K, Haramaty L, Karp CM, White E, Immortalized mouse epithelial cell models to study the role of apoptosis in cancer. Methods Enzymol 446, 77–106 (2008). [PubMed: 18603117]

41. Zhong L, D'Urso A, Toiber D, Sebastian C, Henry RE, Vadysirisack DD, Guimaraes A, Marinelli B, Wikstrom JD, Nir T, Clish CB, Vaitheesvaran B, Iliopoulos O, Kurland I, Dor Y, Weissleder R, Shirihai OS, Ellisen LW, Espinosa JM, Mostoslavsky R, The histone deacetylase Sirt6 regulates glucose homeostasis via Hif1alpha. Cell. 140, 280–93 (2010). [PubMed: 20141841]

42. Schindelin J, Arganda-Carreras I, Frise E, Kaynig V, Longair M, Pietzsch T, Preibisch S, Rueden C, Saalfeld S, Schmid B, Tinevez J-Y, White DJ, Hartenstein V, Eliceiri K, Tomancak P, Cardona A, Fiji: an open-source platform for biological-image analysis. Nat Methods. 9, 676–82 (2012). [PubMed: 22743772]

43. Schneider CA, Rasband WS, Eliceiri KW, NIH Image to ImageJ: 25 years of image analysis. Nat Methods. 9, 671–675 (2012). [PubMed: 22930834]

44. Buescher JM, Antoniewicz MR, Boros LG, Burgess SC, Brunengraber H, Clish CB, DeBerardinis RJ, Feron O, Frezza C, Ghesquiere B, Gottlieb E, Hiller K, Jones RG, Kamphorst JJ, Kibbey RG, Kimmelman AC, Locasale JW, Lunt SY, Maddocks ODK, Malloy C, Metallo CM, Meuillet EJ, Munger J, Nöh K, Rabinowitz JD, Ralser M, Sauer U, Stephanopoulos G, St-Pierre J, Tennant DA, Wittmann C, Heiden MGV, Vazquez A, Vousden K, Young JD, Zamboni N, Fendt S-M, A roadmap for interpreting (13)C metabolite labeling patterns from cells. Curr Opin Biotech 34, 189–201 (2015). [PubMed: 25731751]

45. Mackay GM, Zheng L, van den Broek NJF, Gottlieb E, Methods in Enzymology. Methods Enzymol 561, 171–196 (2015). [PubMed: 26358905]

46. Boon R et al. Amino acid levels determine metabolism and CYP450 function of hepatocytes and hepatoma cell lines. Nature Communications 11, 1393 (2020).

47. Grinde MT et al. Glutamine to proline conversion is associated with response to glutaminase inhibition in breast cancer. Breast Cancer Res 21, 61 (2019). [PubMed: 31088535]

48. Bernasocchi T et al. Dual functions of SPOP and ERG dictate androgen therapy responses in prostate cancer. Nature Communications 12, 734 (2021)

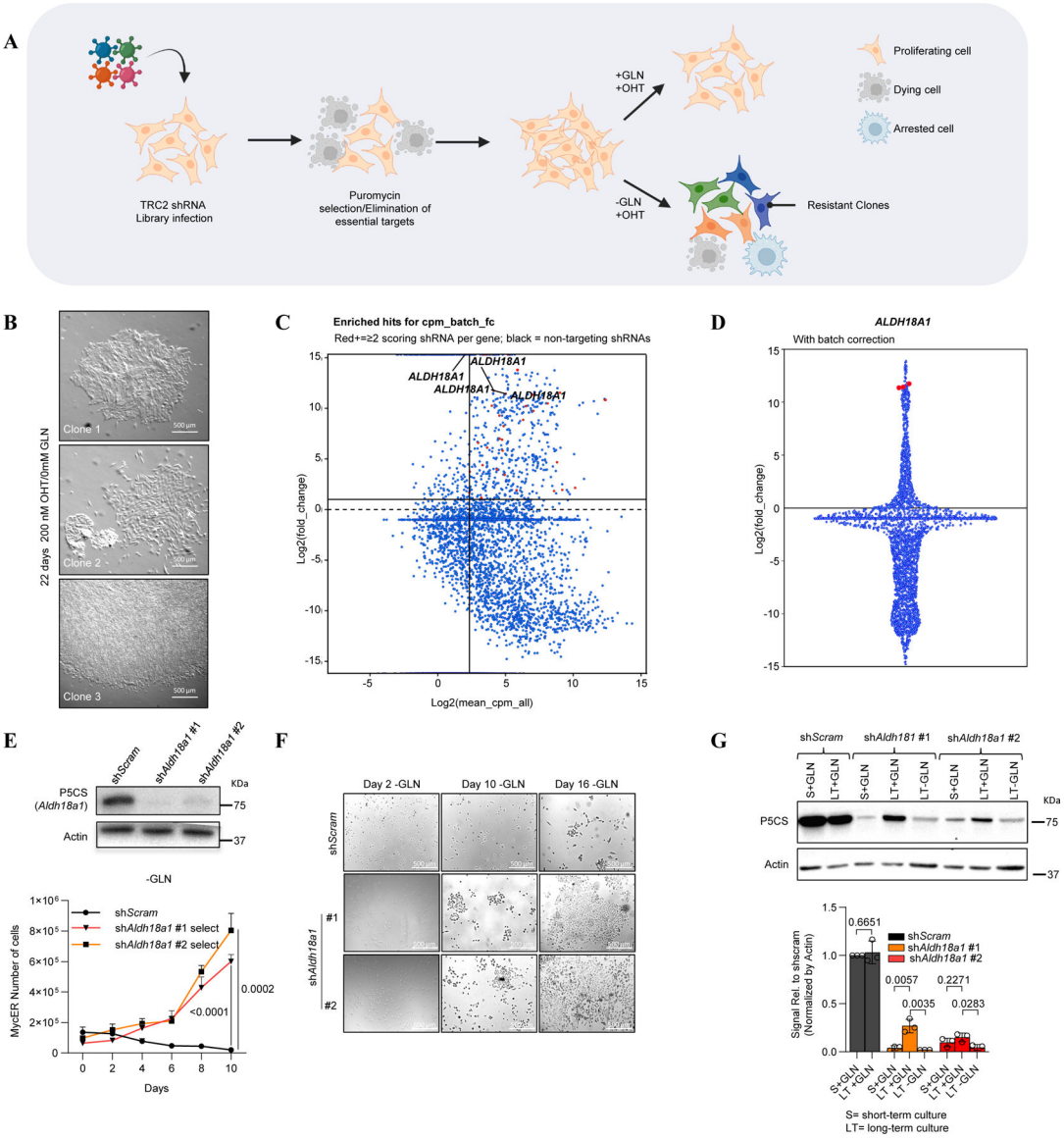

Fig. 1. A genome-wide glutamine deprivation screen identified *Aldh18a1* as a modulator of glutamine metabolism.

A) Graphical representation of glutamine depleted screen, where cells are infected with the TRC2 lentiviral mouse shRNA library, selected, and subjected to glutamine deprivation to select for glutamine independent clones. Created with BioRender.com. **B)** Representative actively proliferating clones arising from the glutamine-deprived KD screen after 22 days of glutamine depletion (n=3). **C)** MA plot of $\log_2$(mean counts-per-million) against $\log_2$(median fold-change) for each shRNA, with points colored red for genes with at least two shRNAs passing thresholds (≥ 5 cpm in control or treatment and fold-change of ≥ 2). Points for all other shRNAs are in grey. Labels indicate positions of shRNAs targeting *Aldh18a1*. **D)** Plot showing distribution of $\log_2$(median fold-change) for all shRNAs (blu) with finite fold-change values, with points horizontally jittered according to density. shRNAs targeting *Aldh18a1* are in red. **E**) In the upper part, western blot of P5CS in MycER MEFs stably expressing a scrambled control short hairpin (shScram) or two independent

short hairpins targeting *Aldh18a1*. In the lower part, cell proliferation of control or *Aldh18a1* knockdown MycER MEFs while grown in glutamine-deprived media for ten days (n=3). P-values were calculated using an unpaired t-test with FDR correction using the Benjamini-Hochberg method. Data are presented as mean values ± SD. **F)** Phase-contrast microscopy of control or *Aldh18a1* knockdown MycER MEFs after 2, 10, and 16 days glutamine deprivation. **G)** representative western blot of P5CS in short-term (S) vs. long-term (LT) culture of shScram and sh*Aldh18a1* MycER MEFs in complete or glutamine deprived media, and corresponding quantification (n=3) Statistical significance was determined using an unpaired, Two-tailed T-Test. Data are presented as mean values ± SD, (n=3).

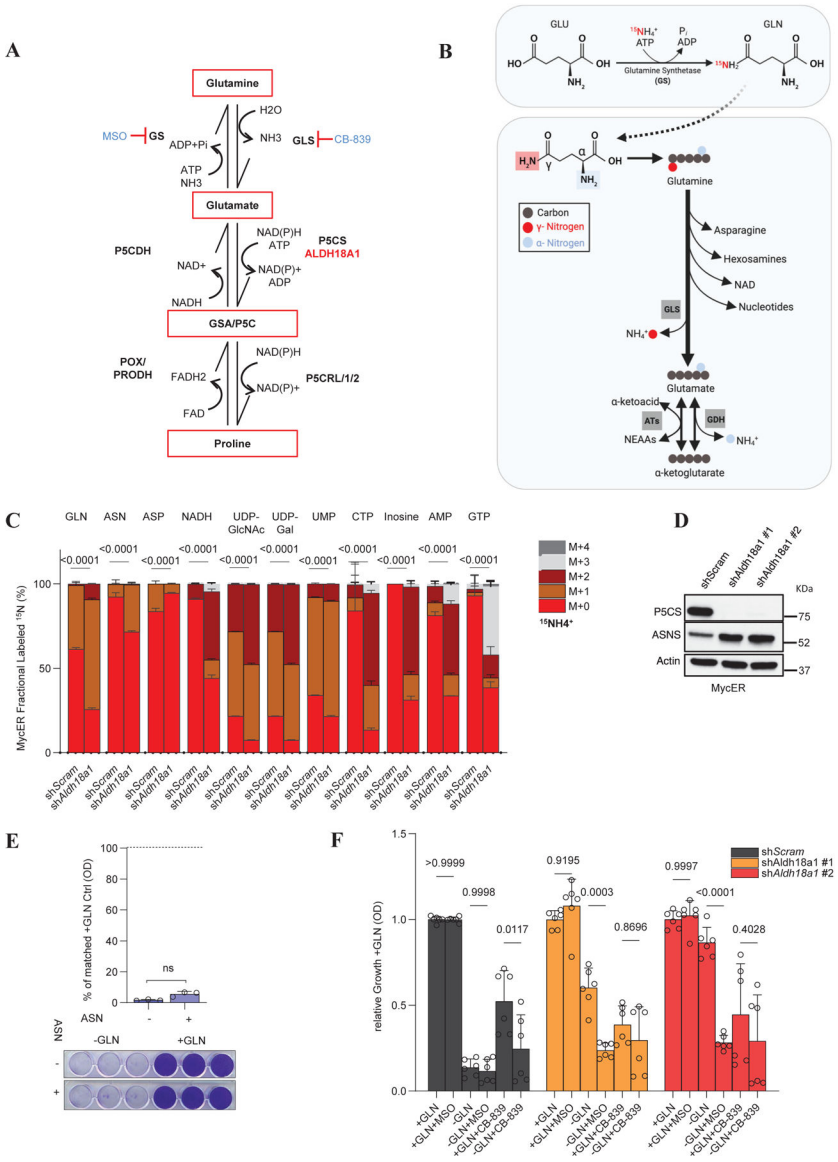

Fig. 2. Decreased *Aldh18a1* expression re-wires cellular metabolism.

A) Graphical representation of the proline biosynthetic pathway, whereby proline is synthesized via glutamate by P5CS, the encoded protein of *Aldh18a1*. **B)** Graphical representation of $^{15}NH_4$ labeling of newly synthesized glutamine, catalyzed by GS, and its utilization for downstream metabolites. **C)** Fractional labeling of select metabolites from samples labeled with $^{15}NH_4Cl$ for 24 hours: glutamine; ASN; ASP; NADH; hexosamines UDP-GlcNAc and UDP-galactose; and nucleotides, UMP, CMP, IMP, and AMP. Statistical significance was determined using 2way ANOVA. Data are presented as mean values ± SD. N=3 biological independent samples. **D)** Western blot of P5CS and ASNS proteins in shScram and sh*Aldh18a1* MycER MEFs. **E)** Crystal violet staining and corresponding quantification of MycER shScram cells cultured in complete or glutamine-deprived media, with or without supplementation of 2mM ASN for 5 days. Statistical significance was determined using a paired, Two-tailed T-Test. Data are presented as mean values ± SD. N=3

biological independent samples. **F)** Bar plot of control or *Aldh18a1* knockdown MycER MEFs while grown in complete or glutamine deprived media, + or – 1mM MSO on + or – 10 μM of CB-839 for 5 days. Statistical significance was determined using two-way ANOVA followed by Tukey's post hoc test for multiple comparisons. Data are presented as mean values ± SD, N=6 biological independent samples.

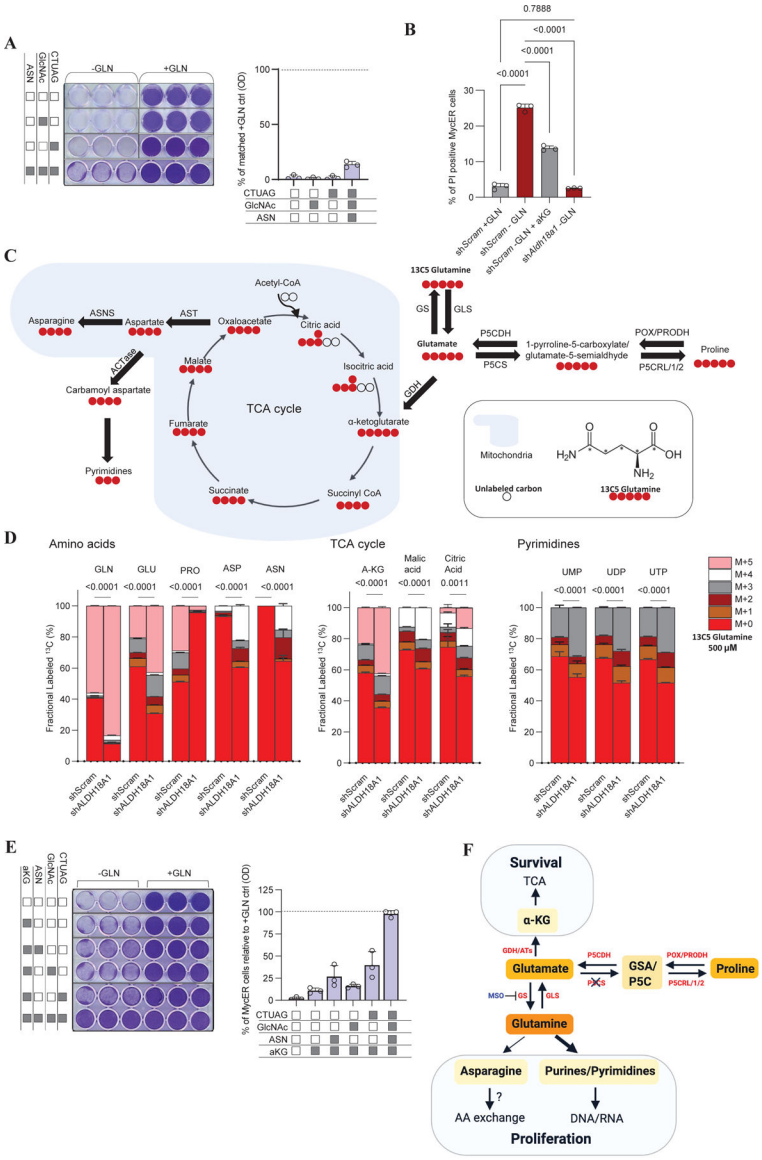

Fig.3. Glutamine biosynthesis allows α-KG dependent survival and nucleotide/asparagine-dependent proliferation in the absence of exogenous glutamine.

A) Crystal violet staining and corresponding colorimetric quantification of MycER shScram cells cultured in complete or deprived, while grown in complete or glutamine deprived media, + or - 2mM ASN, 15mM GlcNAc, or 250µM each cytidine (C), thymidine (T), uridine (U), adenosine (A), and guanosine (G) in indicated combinations for 5 days with corresponding quantification. Data are presented as mean values ± SD. N=3 biological independent samples. **B**) Propidium iodide staining of MycER cells quantified by Flow cytometry. Data are presented as mean ± SD from three independent experiments. Statistical analysis was performed using two-way ANOVA. **C)** Graphical representation of the $^{13}C_5$ glutamine labeling pathway, illustrating its incorporation into intermediates of the TCA cycle, amino acids, and pyrimidines **D)** Tracer experiment using $^{13}C_5$ labeled glutamine in Control and P5CS Knockdown Cells. The bar chart illustrates the proportion of proline derived from glutamine in both control and P5CS knockdown cells,

as well as the corresponding increase in the labeling of amino acids, nucleosides, and TCA cycle intermediates. Data are represented as mean ± SD of three independent experiments. The statistical analysis was performed using two-way ANOVA. **E)** Crystal violet staining and corresponding quantification of MycER shScram cells cultured in complete or deprived media for 5 days. Cells were cultured in DMEM supplemented with 7mM dimethyl-α-ketoglutarate (α-KG), 2mM ASN, 15mM GlcNAc, or 250μM each cytidine (C), thymidine (T), uridine (U), adenosine (A), and guanosine (G) in indicated combinations. Data are presented as mean values ± SD. N=3 biological independent samples. **F)** Model of working hypothesis: *Aldh18a1* deficient cells overcome glutamine dependency by re-routing glutamate away from proline biosynthesis and towards α-KG, ASN, and nucleotide production. Together, these carbon and nitrogen sources support cell survival and proliferation in the context of glutamine-deprived condition. Grey square: Presence ; white square: Absence

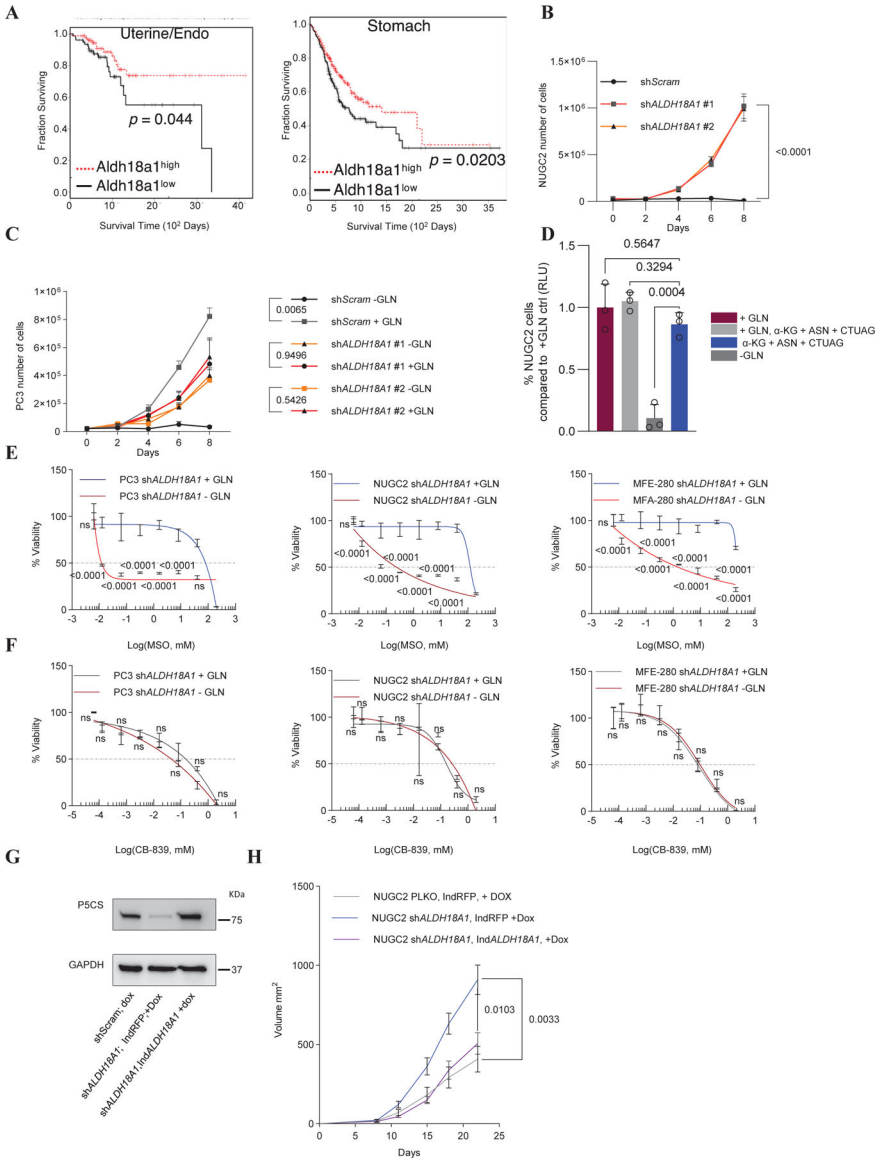

Fig. 4. Downregulation of P5CS in human cancer cells leads to glutamine resistance and increased sensitivity to MSO inhibitor.

A) Kaplan-Meier survival curves analyzing The Cancer Genome Atlas (TCGA) human uterine/endometrial or stomach cancer patient samples based on Aldh18a1 mRNA expression with log-rank p-value (Mantel-Haenszel test) calculated in R with survdiff. **B)** Cell proliferation of control or *ALDH18A1* knockdown NUGC2 cells while grown in glutamine-deprived media for eight days (n=3). Statistical significance was determined using two-way ANOVA followed by Tukey's post hoc test for multiple comparisons. Data are presented as mean values ± SD. **C**) Cell proliferation of control or *ALDH18A1* knockdown PC3 cells while grown in normal or glutamine-deprived media for eight days (n=3). Statistical significance was determined using ordinary one-way ANOVA followed by Tukey's post hoc test for multiple comparisons. Data are presented as mean values ± SD. **D)** Bar plot experiment of NUGC2 cells cultured in complete or glutamine-deprived media for 5 days. Cells were cultured in DMEM supplemented with 3.5mM α-KG, 2mM ASN,

and 125μM each C, T, U, A, and G. Statistical significance was determined using 2way ANOVA, multiple test Turkey. Data are presented as mean values ± SD. N=3 biological independent samples. **E)** Dose-response to MSO inhibitor in various cancer cell lines. From left to right the panel shows the response of PC3, NUGC2, and MFE-280 cell lines to varying concentrations of MSO. Statistical significance was determined using two-way ANOVA followed by Sidak's post hoc test for multiple comparisons. Data are presented as mean values ± SD. N=3 biological independent samples. **F)** Dose-response to CB-839 inhibitor in various cancer cell lines. From left to right the panel shows the response of PC3, NUGC2, and MFE-280 cell lines to varying concentrations of MSO. Statistical significance was determined using two-way ANOVA followed by Sidak's post hoc test for multiple comparisons. Data are presented as mean values ± SD. N=3 biological independent samples. **G)** Western blot analysis of the NUGC2 cell line, comparison between control, sh*ALDH18A1*, and s*hALDH18A1* rescued with exogenous expression of P5CS, (n=3). **H)** line graph representing the progression of tumor volume over time in control (8), sh*ALDH18A1* (8), and in the inducible *ALDH18A1* (8) tumors. Statistical significance was determined using two-way ANOVA followed by Tukey's post hoc test for multiple comparisons. Data are presented as mean values ± SD. N=8 independent animals.

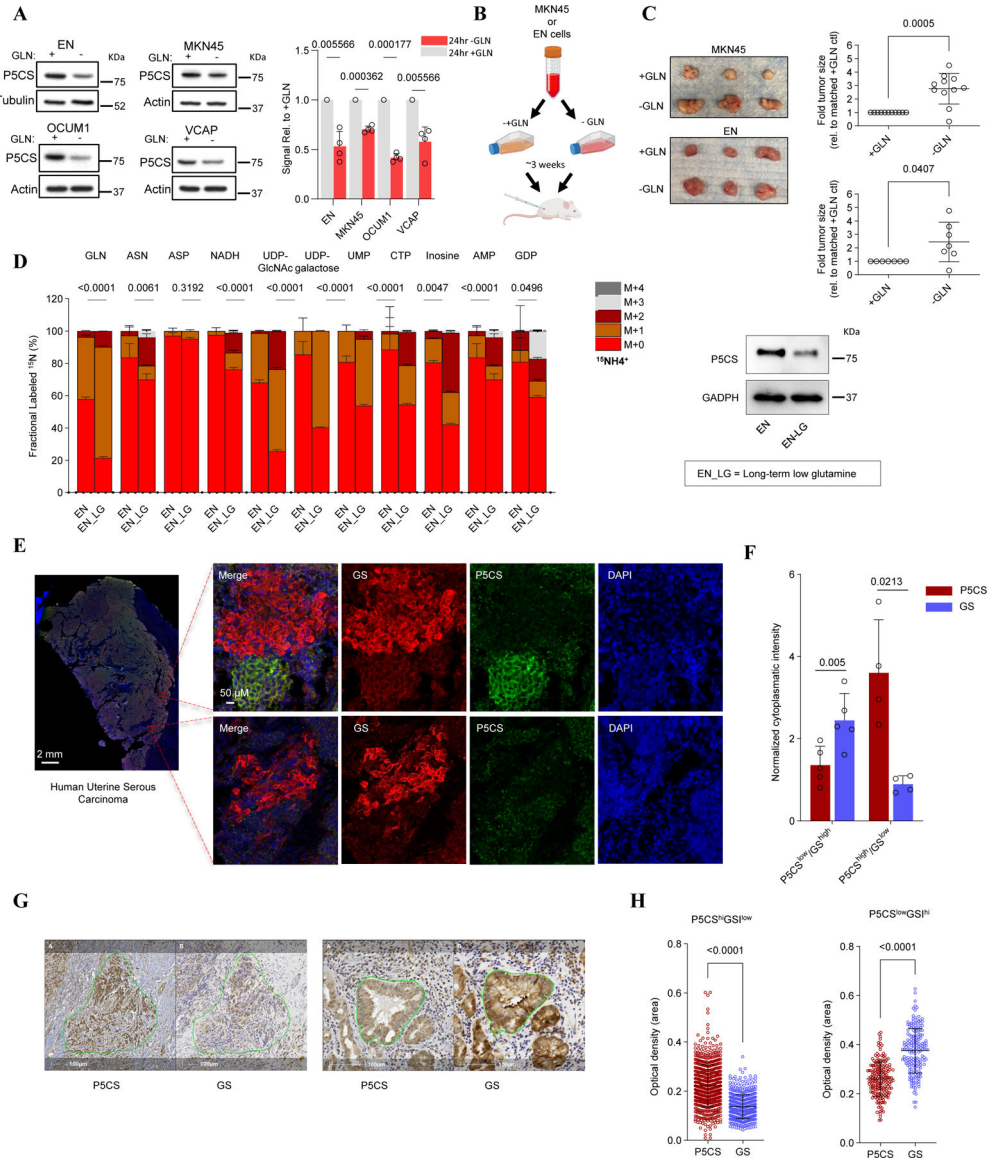

Fig. 5. Human cancer cells reduce P5CS expression as an adaptation to glutamine restriction

A) Representative western blots of P5CS in human cancer cell lines found to endogenously downregulate P5CS upon acute glutamine starvation, with corresponding quantification. EN, MKN45, OCUM1, and VCAP cells were cultured in complete or glutamine-deprived media for 24 hrs (n=3). Statistical significance was determined using an unpaired t-test with Welch's correction for unequal variances, applying individual variance for each group. The False Discovery Rate (FDR) was controlled using the two-stage step-up method by Benjamini, Krieger, and Yekutieli Data are presented as mean values ± SD. **B)** Graphical representation of experimental design: MKN45 or EN cells were cultured in complete or glutamine-deprived condition long term (~ 3 weeks), then injected into matching flanks of SCID mice. Created with BioRender.com. **C)** Representative xenograft tumors removed from SCID mice injected with MKN45 (1×10^6 cells + 20% Matrigel; n=11) or EN (2×10^6+20% Matrigel; n=7) cells cultured in complete or glutamine deprived media (Left).

Tumors were removed at 5 weeks (MKN45) or 6–8 weeks (EN). Fold tumor size, relative to matching +glutamine flank control (Right). Statistical significance was determined using a two-tailed unpaired t-test with Welch's correction for unequal variances. Data are presented as mean values ± SD. **D)** EN and EN_LG (Long-term low glutamine) fractional labeling of select metabolites from samples labeled with $^{15}NH_4Cl$ for 24 hours: GLN (glutamine); ASN (asparagine); ASP (aspartate); NADH; hexosamines UDP-GlcNac and UDP-galactose; and nucleotides, UMP, CMP, IMP, and AMP. Right: immunoblot showing representative image of P5CS levels in control and low glutamine EN cells. Statistical significance was determined using 2way ANOVA. Data are presented as mean values ± SD. N=3 biological independent samples. **E)** Representative immunofluorescence (IF) of a tumor section of uterine serous carcinoma, depicting staining by IF for P5CS (red), GS (green), and Dapi (blue). On the right, a selected area of the tumors demonstrates an inverse correlation between P5CS and GS expression (n=3). **F)** Quantitative analysis of the cytoplasmic intensity of P5CS and GS in the same cells, based on immunofluorescence measurements in five independent tumors. Statistical analysis was performed using a paired, Two-tailed t-test. Data are presented as mean values ± SD. N=5 independent tumors for $P5CS^{low}/GS^{high}$ and respectively N=4 independent tumors for $P5CS^{high}/GS^{low}$. **G)** Examples of immunostaining against P5CS and GS in gastric cancer sections. Note that areas of high P5CS exhibit low GS staining (left image) and *vice versa* (right image). **H)** Quantitative analysis of the samples indicated in J. Data is presented as average optical density (from at least three independent regions) for each marker (n=3). Statistical significance was determined using an unpaired, Two-tailed t-test with a Mann-Whitney test for non-normally distributed data. Data are presented as mean values ± SD, (n=1).